Material characterization by line-focus-beam acoustic microscope

Material Characterization by Line-Focus-Beam Acoustic Microscope

JUN-ICHI KUSHIBIKI, MEMBER, IEEE, AND NORIYOSHI CHUBACHI, MEMBER, IEEE

Abstract—**A novel method of material characterization by means of the line-focus-beam acoustic microscope system with high measurement accuracy is described. The material characterization is carried out by measuring the propagation characteristics of leaky waves on the water–sample boundary; that is, the phase velocity and attenuation are determined through $V(z)$ curve measurements. A general measurement principle is developed to make experimental determination of the two acoustic quantities simultaneously from measured $V(z)$ curves. A spectral analysis method is introduced as a general means to analyze acoustic properties from the $V(z)$ curves. The system is constructed with special software for a signal-processing procedure developed on the basis of the measurement principle. Measurements using a variety of isotropic, as well as anisotropic materials where the velocities extend from 2000 to 11000 m/s, and some other typical samples of layered and membrane structures are reported. All the leaky wave modes, such as leaky surface acoustic wave (SAW), leaky pseudo-SAW, leaky surface-skimming compressional wave, leaky Lamb wave, and harmonic waves, which take part in the interference phenomena in $V(z)$ curves, are investigated. The experimental results are in good agreement with the theoretical results calculated by exact numerical analysis of propagation characteristics of relevant leaky waves. The measurement accuracy is estimated to be about ± 0.2 percent absolute in velocity measurements (less than 0.1 percent for relative measurements) and from a few percent to 20 percent in attenuation measurements. The material characterization method is applied to quantitative investigation of inhomogeneity on wafers and structural analysis of polycrystalline materials.**

I. INTRODUCTION

APPLICATIONS of the acoustic microscope system using a highly focused beam may be divided broadly into two classes to detect microscopic as well as macroscopic acoustic properties of materials; viz., acoustic imaging measurements in the scanning version and quantitative measurements in the nonscanning version. This paper is concerned with the latter class of quantitative measurements of acoustic properties. Material characterization by means of an acoustic microscope using a line-focus beam rather than the point-focus beam employed in more conventional acoustic systems is described.

Since the mechanically scanning acoustic microscope was first developed by Lemons and Quate in 1973 [1], the applications have been widely studied to detect microscopically the variation of acoustic properties of various materials in the fields of biological science, solid material science, and nondestructive evaluation. Developments and improvements of the hardware of the system have also occurred [2]. A major task to advance the research studies has been the interpretation of contrast in the acoustic images. Theoretical analyses of the angular spectrum of the acoustic field have been used to explain the contrast mechanism [3]–[6]. On comparing the theoretical with the experimental results, which were obtained especially for solid materials by the reflection acoustic microscope, it has been found that the output of a piezoelectric transducer varies markedly with distance between the acoustic probe and samples [3]. The record of this output has been called the $V(z)$ curve and is a function of the distance z. As the shapes of the $V(z)$ curves are unique and characteristic of solid materials, it has been pointed out that the reflection acoustic microscope system, operating in the nonscanning mode, provides for the determination of acoustic properties in solid materials [3].

Weglein reported the periodicity of the dips appearing in the $V(z)$ curves in 1979 [7]. As a result of measuring the dip intervals for a variety of solid samples with a wide velocity range, it was established experimentally that the periodic intervals in $V(z)$ curves are closely related to the Rayleigh surface wave velocity on the surface plane of materials. Subsequently, the relationship between the dip interval and Rayleigh wave velocity was established by refining the physical model for the interference phenomena in $V(z)$ curves by Parmon and Bertoni [8] and Atalar [9]. This had great significance because it allows the possibility of quantitative measurements of acoustic properties in microscopic areas using acoustic microscopy.

In the recent rapid development of acoustic microscopy, the $V(z)$ curves have played a very important role for both acoustical imaging and quantitative measurements. As regards acoustical imaging measurements, the curves have been effectively employed, for example, in the interpretation of contrast in acoustic images [2]–[6], [10]–[13] and in image signal processing techniques for obtaining false-color micrographs, which show the internal construction of semiconductor devices [14]. In some cases the measurement of leaky surface acoustic waves (LSAW) propagating on samples has also been used for

Paper received May 1984; revised November 1984. This work was supported in part by the Research Grant-in-Aids, Ministry of Education, Science and Culture and in part by the Toray Science and Technology Grants.

The authors are with the Department of Electrical Engineering, Tohoku University, Sendai 980, Japan.

0018-9537/85/0300-0189$01.00 © 1985 IEEE

quantitative interpretation of the differences in the acoustic contrast. So far, in quantitative measurements, only the velocity of leaky SAW's has been extracted from the $V(z)$ curves. Recently, the attenuation of the relevant waves propagating on samples has been attempted to be extracted from the $V(z)$ curves [15], [16]. Attenuation also provides important information on the acoustic properties of materials, which could be influenced by the water loading factor on samples; the acoustic absorption factor in bulk properties; and structural factors such as surface roughness and the material structure of grains, pores, and boundaries. Thus the two parameters of velocity and attenuation allow complete material characterization on a microscopic scale and the interpretation of the acoustic contrast. In acoustic microscopy the $V(z)$ curve has thus been recognized as an indispensable method for acoustical imaging measurements.

However, the use of these $V(z)$ curves for quantitative measurements of the acoustic properties of materials—which are obtained by the nonscanning reflection acoustic microscope system (using a spherical lens with which a plane wave radiating from the transducer is circularly focused into a point)—has in principle a serious difficulty; that is, the point-focus beam excites leaky SAW's propagating in all directions, so that the acoustic properties are measured as a mean value around the beam axis. This means that the system cannot be applied appropriately for detecting the acoustic properties that reflect crystallographic anisotropies.

An acoustic line-focus beam was proposed to solve this serious problem by the present authors in 1981 [17]. This is realized using a sapphire lens with a cylindrical concave surface. The detection of acoustic anisotropy has been successfully demonstrated for some typical single crystals such as sapphire [18], lithium niobate [19], and silicon [20]. A strict theoretical analysis has been applied to the curves so that numerical calculations have coincided surprisingly well with experimental $V(z)$ curves [21]–[23]. The effects of leaky wave parameters, i.e., velocity and attenuation, on $V(z)$ curves have been clarified by theoretical considerations [24]. Furthermore, fundamental studies on the quantitative measurement mechanism have been made. These studies include the elucidation of the multimode interference mechanism in $V(z)$ curves [25]; the introduction of fast Fourier transform (FFT) analysis for $V(z)$ curves deformed in the dip interval and shape [26]; and the development of a novel measurement principle of determining both velocity and attenuation of leaky waves directly from measured $V(z)$ curves [27].

This paper is the first full treatment describing systematically the material characterization by means of the line-focus-beam acoustic microscope. The principle of material characterization is presented in Section II. A principle for measuring both the velocity and the attenuation of relevant leaky waves directly from $V(z)$ curves is established by adopting a simple representation for the transducer output of $V(z)$, which is approximately constructed by combination of ray and field theories. The measurement principle is expanded to the $V(z)$ curves deformed by multimode interference. On the basis of the principle, a spectral analysis technique is introduced as a general means for analyzing acoustic properties from $V(z)$ curves. We describe the realization of the acoustic line-focus beam using a sapphire lens with a cylindrical concave surface of 1.0-mm radius and examine the performance and the acoustic fields in water at a frequency around 200 MHz in Section III. With use of the lens, the line-focus-beam acoustic microscope system is constructed with software from a signal-processing procedure to determine the acoustic property. In order to verify the material characterization method, the description of experiments performed for a variety of isotropic and anisotropic materials and some other typical samples of layered and membrane structures appears in Section IV. Investigations of all leaky wave modes associated with the interference phenomena in the $V(z)$ curves such as leaky SAW, leaky pseudo-SAW (LPSAW), leaky surface-skimming compressional wave (SSCW), leaky Lamb wave, and harmonic modes of leaky waves are discussed. Important problems that take into account such applications of the system as the method of the utilization, the measurement accuracy, and the limitation of application are discussed in Section V. Two promising applications of the method are presented in Section VI; one is nondestructive testing of acoustic inhomogeneities on wafers such as a gadolinium gallium garnet (GGG) and a lead zirconate titanate (PZT) ceramic, and the other is structural analysis of polycrystalline Mn–Zn ferrites with grains. Conclusions are presented in Section VII.

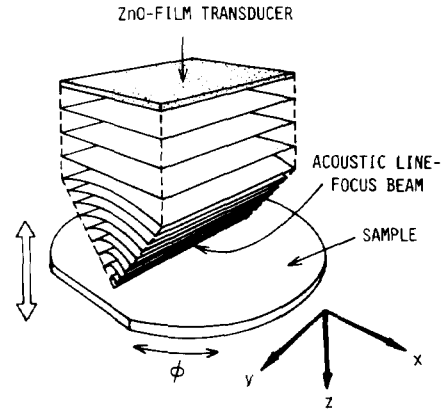

Fig. 1. Illustration of material characterization method by the line-focus-beam acoustic microscope.

II. Principle of Material Characterization

Material characterization by measuring such acoustic properties as sound velocity and attenuation (including anisotropy) can be made in the nonscanning mode of a reflection acoustic microscope using a line-focus beam. The experimental procedure is illustrated conceptually in Fig. 1. The acoustic probe and the sample target are translated relatively along the z-axis direction (beam axis), without scanning in the x and y directions. The

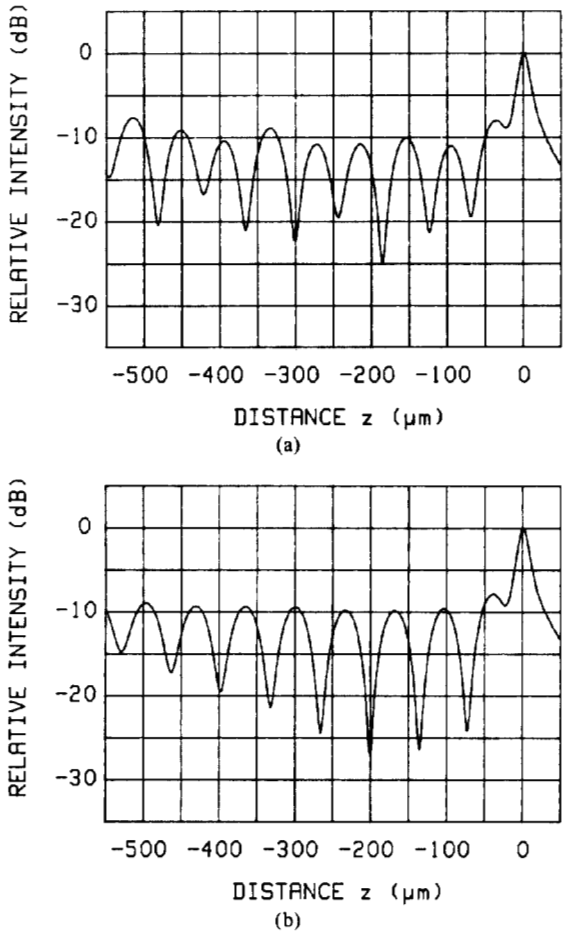

Fig. 2. Typical $V(z)$ curves on water/(111)-Si measured with acoustic line-focus beam at 225 MHz. (a) $\phi = 0°$ ([110]). (b) $\phi = 30°$ ([112]).

acoustic line-focus beam is a wedge-shaped beam with a cylindrical wavefront. The beam is formed by an acoustic lens with a cylindrical concave surface and is linearly focused along one axis on the specimen. The beam is coupled normally to the sample through a coupling liquid that typically consists of distilled water (not shown in the figure). The determination of acoustic properties and anisotropy of materials is made through $V(z)$ curve analysis. $V(z)$ curves are records of signal variations in the piezoelectric transducer output as a function of distance along the z axis. A typical $V(z)$ curve is shown in Fig. 2 as an example, where the transducer output gives a maximum at the distance of $z = 0$ (focal point) and exhibits dips (minima) periodically in the negative z region. This $V(z)$ curve variation is caused by the interference of two components of the acoustic waves detected by the transducer; i.e., one component is associated with the waves near the z axis directly reflected from the sample, and the other component is associated with the waves reradiated from the sample into water through leaky acoustic waves (typically, leaky SAW) excited on the water–sample boundary. In other words the measured $V(z)$ curves contain unique acoustic information relating to the characteristics of leaky waves existing at the water/sample boundary. In Fig. 1 it is shown that, as the beam is focused linearly

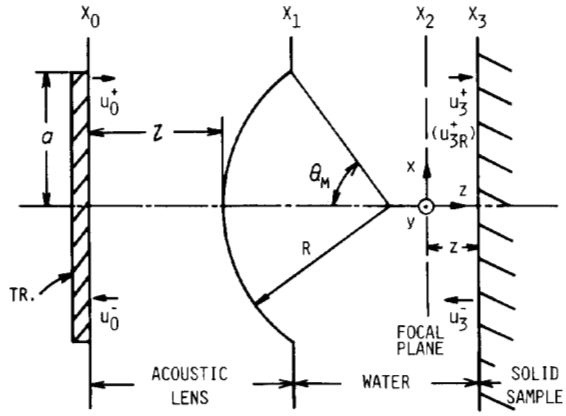

Fig. 3. Cross-sectional geometry of acoustic line-focus-beam lens and coordinate system used for analysis.

along the y-axis direction where $\phi = 0$, the acoustic property of leaky waves propagating in the x-axis direction can be recorded with the $V(z)$ curve. For an anisotropic sample, the $V(z)$ curve measurements are performed by rotating the sample about the z axis so that variations in acoustic properties for leaky waves can be obtained as a function of wave-propagation direction.

A. Mathematical Representation for $V(z)$ Curves

Before the measurement procedure is discussed in detail, let us consider the mathematical representation for $V(z)$ curves, which is obtained by the acoustic line-focus beam, in order to understand generally the transducer output. The expressions for the $V(z)$ curves are given briefly in the following section [21] and are derived from the Fourier optics approach, from which the procedure was introduced into acoustic microscopy by Atalar [4] and Wickramasinghe [5].

Fig. 3 shows the cross-sectional geometry for analyzing the $V(z)$ curves. Analysis is made in the two-dimensional xz plane assuming that the acoustic fields do not vary in the y direction since the acoustic-focused fields have a phase structure of cylindrical symmety. In the figure a is the halfwidth of transducer; l is the distance between the transducer and the top surface of the lens; and R and θ_M are the radius of curvature and the half-aperture angle for the acoustic lens, respectively. The origin of the coordinate system (x, y, z) is placed at the focal point for the acoustic fields in water. Coordinates x_0, x_1, x_2, and x_3 are placed at the transducer, the acoustic lens, the focal, and the sample planes, respectively. For a simple description x_1 is on the acoustic lens plane. There is a Fourier transform relationship between the position x in planes parallel to the sample surface, and the spatial frequency k_x, where k_x is the x component of the wavenumber k_w in the coupling liquid. The final form of the transducer output is represented as follows:

$$V(z) = A \int_{-\infty}^{\infty} u_{3R}^{+}(x_3) \cdot u_3^{-}(x_3)\, dx_3, \qquad (1)$$

where A is the arbitrary amplitude constant. The refer-

ence field distribution $u_{3R}^{+}(x_3)$ and the reflected field distribution $u_3^{-}(x_3)$ are defined at the sample plane, respectively, as follows:

$$u_{3R}^{+}(x_3) = \{T^{-}(x_1)/T^{+}(x_1)\} \cdot u_3^{+}(x_3) \tag{2}$$

and

$$u_3^{-}(x_3) = F^{-1}\{R(k_x, \phi) \cdot F\{u_3^{+}(x_3)\}\}. \tag{3}$$

The $u_3^{+}(x_3)$ is the incident field distribution at the sample plane. The quantities $T^{+}(x_1)$ and $T^{-}(x_1)$ are the transfer coefficients from lens to water and from water to lens at the lens plane, respectively, and include the effect of the acoustic antireflection coating layer. The function of $R(k_x, \phi)$ represents the reflectance function for reflecting the elastic information of materials at the water–sample boundary, in which ϕ is the wave propagation direction under consideration. The distribution of $u_3^{+}(x_3)$ is given by

$$u_3^{+}(x_3) = F^{-1}\{F\{u_2^{+}(x_2)\} \cdot \exp(jk_z z)\}, \tag{4}$$

where $u_2^{+}(x_3)$ is the incident field distribution at the focal plane, and k_z is the z component of the wavenumber k_w for the longitudinal wave in water, defined as $k_z = (k_w^2 - k_x^2)^{1/2}$. The incident acoustic field has spatial frequency components ranging from 0 to k_x, which is limited by the aperture angle of the acoustic lens shown in Fig. 3. The spectrum distribution depends on the geometric dimensions of the acoustic line-focus-beam lens and transducer and the operating frequency f. The symbols F and F^{-1} denote the Fourier transform and the inverse Fourier transform, respectively.

Thus the transducer output of $V(z)$ obtained with the line-focus beam is represented by the reference field distribution $u_{3R}^{+}(x_3)$, which is determined uniquely by the acoustic lens, and the reflected field distribution $u_3^{-}(x_3)$, which contains the acoustic response of the materials to be measured. The shapes of the $V(z)$ curves are essentially dominated by the reflectance function $R(k_x, \phi)$ of the materials. They also depends strongly on the wave propagation direction ϕ, when the material is anisotropic around the z axis.

B. Analysis of $V(z)$ Curves

The field theory described cannot guide the direct measurement procedure for extracting acoustic properties from the measured $V(z)$ curves. In order to establish this procedure, we first require an approximate simple expression for $V(z)$ curves. Here we simplify the representation of $V(z)$, based on the following four important facts that have emerged from the theoretical and experimental studies on the $V(z)$ curve measurements.

1) A simple interference model by ray theory has been recognized for the determination of characteristics of leaky waves that propagate on the boundary of water and samples [7]–[9], [18]–[23]. The velocity is calculated from the periodic dip interval appearing in the $V(z)$ curves obtained by both the point-focus beam and the line-focus beam.

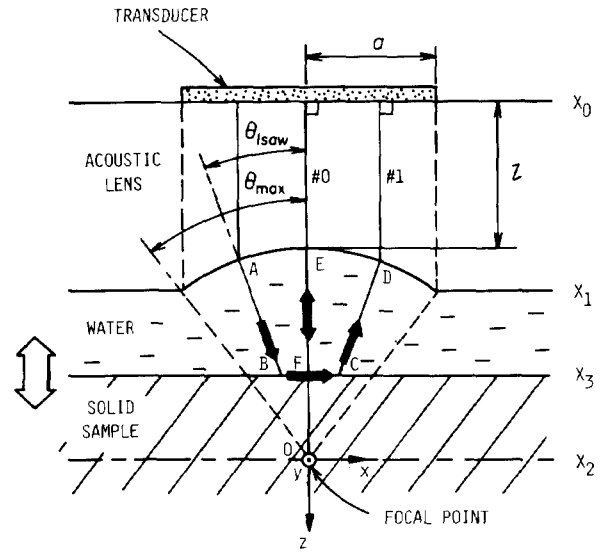

Fig. 4. Cross-sectional geometry of acoustic line-focus-beam lens, explaining the construction mechanism of $V(z)$ curves and constituting the material characterization method.

2) The numerical calculations of $V(z)$ curves with parameters for the acoustic line-focus-beam lens employed in experiments can explain extremely well both the shape and the dip interval of the measured $V(z)$ curves [21], [23].

3) The numerical calculations have given a general interpretation of the effect of leaky wave parameters, viz., phase velocity and attenuation factor, on the $V(z)$ curve measurements by introducing an ideal reflectance function, where only the propagation characteristics of the leaky wave are taken into account [24]. The velocity determines the interval of dips in $V(z)$ curves, while the attenuation factor affects the shape of $V(z)$ curves.

4) There is an excellent agreement between the acoustic tic properties derived from measurement and the theoretical results obtained by the exact numerical calculations for leaky waves on the boundary of water and samples [18]–[20], [23].

1) Measurement Principle: Fig. 4 shows schematically the cross-sectional geometry of the acoustic line-focus beam. Coordinate (x, y, z) is set at the focal plane in water. A sample is illuminated with focused acoustic fields having wide spatial frequency spectra limited by the angle θ_{max}. Now, let us consider the simplest case of one leaky wave mode (here a leaky SAW). The wave can be excited by the acoustic line-focus beam when the critical angle θ_{LSAW} is less than the angle θ_{max}. There is a simple model of interference in the transducer output of $V(z)$ detected at the ZnO transducer. One component (#0) constitutes the acoustic waves near the z axis directly reflected from the sample, and another component (#1) is associated with the waves reradiated from the sample via the leaky SAW existing on the boundary. The latter waves correspond to a portion of the reradiated waves propagating on the boundary the distance $\overline{BC}$. The remaining reradiated waves can not effectively reach the transducer due to refraction at the lens surface. The transducer out-

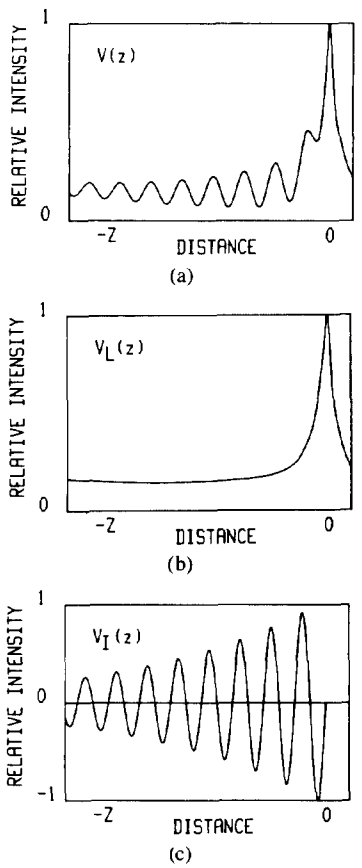

Fig. 5. Decomposition of $V(z)$ curve.(a) $V(z)$. (b) $V_L(z)$. (c) $V_I(z)$.

put $V(z)$ is expressed as a combination of these two components. The transducer output $V(z)$ is expressed as a combination of these two components. The major components contributing to the $V(z)$ curve are shown conceptually in Fig. 5. We now assume that the entire transducer output $V(z)$ can be approximately represented by combining ray theory for the leaky SAW component and field theory for the directly reflected component in the negative z region as

$$V(z) = V_I(z) + V_L(z), \tag{5}$$

where $V_L(z)$ (see Fig. 5(b)) is the characteristic lens response defined as the hypothetical transducer output with respect to z, which is derived by field theory, and where the response for the leaky SAW component (#1) is completely excluded. The lens response $V_L(z)$ depends uniquely on the dimensions of the acoustic line-focus-beam lens and the operating frequency, namely, acoustic field distribution. The amplitude of $V_L(z)$ is maximum when the sample is located at the focal point ($z = 0$) because the transducer can receive acoustic waves with almost all of the spatial frequency components reflected from the sample. As the sample is moved towards the lens along the z axis, wave components with lower spatial frequencies around the beam axis will be dominantly received by the transducer, so that the amplitude abruptly decreases and becomes almost constant.

The function $V_I(z)$ is derived by ray theory and mathematically describes the interference of the two components #0 and #1 defined previously, where the $V_L(z)$ is used as a reference signal. We can derive the expression for $V_I(z)$ by considering two different propagation paths. The translation of the sample by a distance z from the focal plane to the lens gives rise to phase variations $\zeta_0(z)$ for #0, and $\zeta_1(z)$ for #1 as follows (see Fig. 4):

$$\zeta_0(z) = -2 \cdot \overline{OF} \cdot k_w = -2k_w z \tag{6}$$

$$\begin{aligned}\zeta_1(z) &= -\overline{BOC} \cdot k_w + \overline{BC} \cdot k_{\mathrm{LSAW}} \\ &= -2k_w z/\cos\theta_{\mathrm{LSAW}} \\ &\quad + 2k_{\mathrm{LSAW}} \cdot z \cdot \tan\theta_{\mathrm{LSAW}}.\end{aligned} \tag{7}$$

So the relative phase change ξ between a #0- and #1-per-unit translation distance z is given by

$$\begin{aligned}\xi &= (\zeta_1(z) - \zeta_0(z))/z \\ &= 2(k_w(1 - 1/\cos\theta_{\mathrm{LSAW}}) + k_{\mathrm{LSAW}} \cdot \tan\theta_{\mathrm{LSAW}}),\end{aligned} \tag{8}$$

where $k_w = 2\pi f/v_w$, $k_{\mathrm{LSAW}} = 2\pi f/v_{\mathrm{LSAW}}$, and $\theta_{\mathrm{LSAW}} = \sin^{-1}(v_w/v_{\mathrm{LSAW}})$. The quantity v_w is the longitudinal velocity in water, viz., $v_w = 1483$ m/s at 20°C [28], and v_{LSAW} is the phase velocity of the leaky SAW on the boundary. The initial phase difference ψ between #0 and #1 at the focal plane can be calculated in a similar way by additionally taking into account the phase variation of π [29], which occurs on reflection at the critical angle θ_{LSAW} for the leaky SAW

$$\begin{aligned}\psi &= 2(\overline{OE} - \overline{OA} \cdot \cos\theta_{\mathrm{LSAW}})k_s \\ &\quad + 2\overline{OA} \cdot k_w + \pi - 2\overline{OE} \cdot k_w \\ &= 2f_l(k_s - k_w) + 2t(0) \\ &\quad \cdot (k_w - k_s \cdot \cos\theta_{\mathrm{LSAW}}) + \pi,\end{aligned} \tag{9}$$

where $k_s = 2\pi f/v_s$ in which v_s is the longitudinal velocity in a sapphire lens, f_l ($=\overline{OE}$) is the focal length, and the function $t(z)$ ($=\overline{AB}$) is as a function of z. For rays of both the #0 and #1 paths, considering the attenuation coefficient α_w in water ($\alpha_w/f^2 = 25.3 \times 10^{-17}$ s^2/cm [30]), and the attenuation (ATT) factor of leaky SAW propagating on the boundary, we can represent the $V_I(z)$ as

$$V_I(z) = C \cdot \mathrm{ATT} \cdot \exp(j(\xi z + \psi)), \tag{10}$$

where

$$\mathrm{ATT} = \exp(-2\alpha_w t(z)) \cdot \exp(2\gamma z \cdot \tan\theta_{\mathrm{LSAW}}), \tag{11}$$

$$\gamma = 2\pi f\alpha/v_{\mathrm{LSAW}}, \tag{12}$$

$$\alpha = \alpha_{\mathrm{LSAW}} + \alpha_b + \alpha_s. \tag{13}$$

The quantities α_{LSAW}, α_b, and α_s are the normalized attenuation factors due to the water loading effect, the acoustic bulk absorption effect, and structural scattering effects, respectively. The amplitude constant C depends on the acoustic field distribution and the excitation efficiency for a leaky SAW.

A phase change of 2π in the relative phase difference

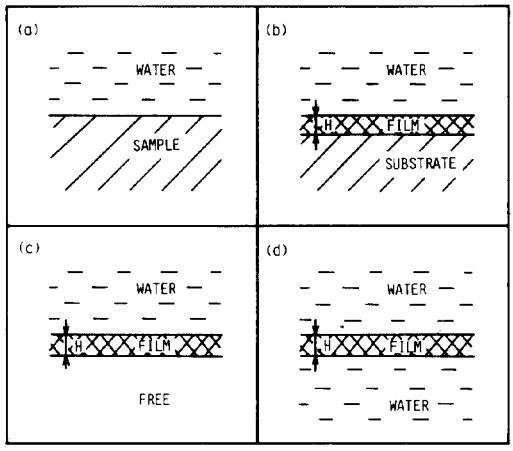

Fig. 6. Sample configurations to be characterized by the line-focus-beam acoustic microscope.

$\zeta_0(z) - \zeta_1(z)$, corresponds to the dip interval Δz in $V(z)$ curves. Using (8), we can obtain

$$\Delta z = v_w/2f(1 - \cos \theta_{\mathrm{LSAW}}). \tag{14}$$

Equation (14) can be also represented in terms of v_{LSAW} as

$$v_{\mathrm{LSAW}} = v_w/(1 - (1 - v_w/2f\Delta z)^2)^{1/2}. \tag{15}$$

Thus, this simplified theory representing the $V(z)$ curves states that, if the $V_I(z)$ function is extracted from experimental data, we can determine directly the two physical quantities, namely the velocity and the attenuation of a leaky SAW, from (10)–(15). The velocity is determined from the dip interval Δz of the interference and the attenuation from the gradient of the interference amplitude.

The experimental procedure is given as follows:

a) record the $V(z)$ curves;
b) extract $V_I(z)$ from $V(z) - V_L(z)$;
c) determine v_{LSAW} from $V_I(z)$;
d) measure ATT from $V_I(z)$; and,
e) determine of γ and α from ATT.

2) Multiple Modes: The measurement procedure for material characterization developed above will be applicable to four kinds of representative configurations as illustrated in Fig. 6: (a) for semi-infinite samples for which the thickness is much greater than the wavelength of a leaky wave; (b) for samples with thin-film-layered or diffusion-layered structures; and (c) and (d) for thin-film samples for which there are two cases of water-loading, on one side and on both sides. In each case we should generally take into account some other leaky modes; i.e., leaky pseudo-SAW mode [20], [25], [26], leaky surface skimming compressional wave mode [7], leaky Lamb wave mode [31], [32], and harmonic modes of leaky waves, in addition to a fundamental leaky SAW mode on the boundary. If multiple leaky waves could be excited efficiently on the boundary, they would take part in the interference phenomena in $V(z)$ curves. So, here we will develop a more general measurement principle.

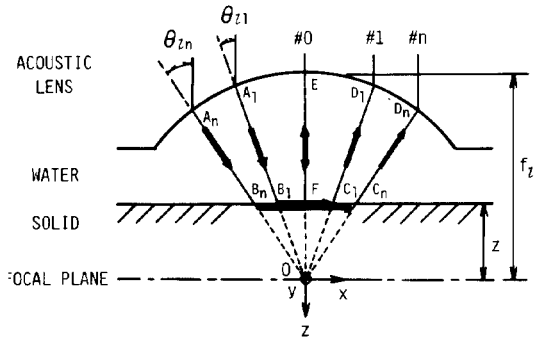

Fig. 7. Cross-section of acoustic line-focus beam to explain the multimode interference mechanism in $V(z)$ curves.

Fig. 7 shows the cross section of acoustic line-focus beam used to explain the interference mechanism for multiple leaky waves in $V(z)$ curves. Each mode is excited at its critical angle $\theta_l(n)$ by the focused acoustic waves and propagates with its characteristic phase velocity $v_l(n)$ and attenuation $\alpha(n)$ on the boundary. Specifically, we can represent the interference output $V_{In}(z)$ between #0 and #n as before

$$V_{In}(z) = C(n) \cdot \mathrm{ATT}\ (n) \cdot \exp\ (j(\xi(n)z + \psi(n))). \tag{16}$$

Now, we assume that the construction mechanism for $V(z)$ curves is a linear system, so that we can take a superpositional model for the total interference output $V_I(z)$ as

$$V_I(z) = V_{I1}(z) + V_{I2}(z) + \cdots + V_{In}(z). \tag{17}$$

The final expression for $V(z)$ is given by

$$V(z) = \Sigma V_{In}(z) + V_L(z). \tag{18}$$

The characteristic lens response $V_L(z)$ is the same function as for the single leaky mode in (5).

As stated above, the measurement principle has been expanded to explain multimode interference in $V(z)$ curves. The efficient excitation of the multiple leaky waves on the boundary results in the deformation of the periodicity of dips and the shape of the characterization region in $V(z)$ curves [25], [26]. It would appear that it might be difficult to determine the acoustic properties of materials using the same simple procedure described in the previous Section II-B-1. The representation of a simple superpositional model of elemental $V_{In}(z)$ curves corresponding to each leaky wave mode suggests that the application of spectrum analysis, such as the FFT, as a general means for analyzing the acoustic property for each mode of materials.

C. Spectral Analysis of Acoustic Properties

Here we introduce a spectral analysis method for the $V(z)$ curves where finite sampled-data waveforms are used.

The Fourier transform for the $V_{In}(z)$ function that was truncated by a rectangular window function with a width

of $2z_w$ is given as follows:

$$F(k) = \frac{1}{2\pi}\int_{-z_w}^{z_w} C(n)\cdot\exp(\alpha_0(n)\cdot z)\cdot\exp(j(\xi(n)z+\psi(n)))\cdot\exp(-jkz)\cdot dz = X_r(k)+jX_i(k), \quad (19)$$

where

$$X_r(k) = \frac{1}{\pi}\cdot\frac{C(n)}{(k-\xi(n))^2+\alpha_0^2(n)}\cdot(\alpha_0(n)A+(k-\xi(n))B) \quad (20)$$

$$X_i(k) = \frac{1}{\pi}\cdot\frac{C(n)}{(k-\xi(n))^2+\alpha_0^2(n)}\cdot(\alpha_0(n)B-(k-\xi(n))A) \quad (21)$$

$$A = \cos\psi(n)\cdot\cos((k-\xi(n))z_w)\cdot\sinh(\alpha_0(n)z_w) - \sin\psi(n)\cdot\sin((k-\xi(n))z_w)\cdot\cosh(\alpha_0(n)z_w) \quad (22)$$

$$B = \sin\psi(n)\cdot\cos((k-\xi(n))z_w)\cdot\sinh(\alpha_0(n)z_w) + \cos\psi(n)\cdot\sin((k-\xi(n))z_w)\cdot\cosh(\alpha_0(n)z_w) \quad (23)$$

$$\alpha_0(n) = -2(\alpha_w/\cos\theta_l(n) - \gamma(n)\cdot\tan\theta_l(n)). \quad (24)$$

The voltage spectrum is defined as

$$|F(k)| = (X_r^2(k)+X_i^2(k))^{1/2}. \quad (25)$$

Now, in order to relate the analyzed spectrum distribution to acoustic quantities, we take note of two spectral components at $k = \xi(n)$ and $\xi(n)+\pi/z_w$ (or $\xi(n)-\pi/z_w$) as given by

$$|F(\xi(n))| = \frac{C(n)}{\pi}\cdot\frac{\sinh(\alpha_0(n)z_w)}{\alpha_0(n)} \quad (26)$$

$$\left|F\left(\xi(n)\pm\frac{\pi}{z_w}\right)\right| = \frac{C(n)}{\pi}\cdot\frac{\sinh(\alpha_0(n)z_w)}{\{(\pi/z_w)^2+\alpha_0^2(n)\}^{1/2}}. \quad (27)$$

Eliminating the function $\sinh(\alpha_0(n)z_w)$ with (26) and (27), we can obtain the following

$$\alpha_0(n) = \frac{\left(\frac{\pi}{z_w}\right)\cdot\left|F\left(\xi(n)\pm\frac{\pi}{z_w}\right)\right|}{\left\{|F(\xi(n))|^2-\left|F\left(\xi(n)\pm\frac{\pi}{z_w}\right)\right|^2\right\}^{1/2}}. \quad (28)$$

The attenuation $\alpha_0(n)$ for the interference output can be imated from the two spectra. Then, using (24), the attenuation factor for the leaky wave on the boundary can be calculated by

$$\gamma(n) = \frac{\alpha_0(n)\cdot\cos\theta_l(n)+2\alpha_w}{2\sin\theta_l(n)}. \quad (29)$$

From a center frequency $\xi(n)$ (mode spectrum) giving a maximum amplitude in spectra, we can measure the dip interval $\Delta z(n)$ in the $V(z)$ curve using the equation

$$\Delta z(n) = 2\pi/\xi(n). \quad (30)$$

Substituting the value $\Delta z(n)$ into (15), we can determine the phase velocity $v_l(n)$ for the leaky wave. Further, using the measured values of $v_l(n)$, $\alpha_0(n)$, and (29) and (12), we can finally determine the normalized attenuation factor $\alpha(n)$ for the nth leaky wave mode.

In general, applying spectral analysis to the $V(z)$ curves where multiple leaky waves contribute, we can determine simultaneously the acoustic quantities of a pair of $v_l(n)$ and $\alpha(n)$ for each leaky wave mode.

D. Discussion

At the same time as we apply the principle described above to measurements for material characterization, we should discuss the following two important factors: the characteristic lens response $V_L(z)$ and the physical properties of distilled water.

In order to proceed with the present measurement procedure, the $V_L(z)$ curve plays a very important role in the principle and affects greatly the measurement accuracy. There are two useful methods for obtaining the $V_L(z)$ curve: the synthesis of the $V_L(z)$ curve from measured $V(z)$ curves using filtering techniques such as digital or analog low-pass filters; and the use of $V(z)$ curves measured for specified samples on which no leaky waves exist or the waves are not so efficiently excited. For example, as the line-focus-beam sapphire lens employed in experiments has an angle of $\theta_{max} = 53°$ in water as shown in Fig. 4, it is desired that the velocity for the fastest leaky wave mode, namely, leaky SSCW, is smaller than or near to the value of $v_l = 1858$ m/s. Possible material choices include Pb [33], Hg [34], vitreous As_2Se_3 [35], and Se [36].

In the present quantitative measurements, distilled water is employed as the reference material with the longitudinal velocity v_w and the attenuation coefficient α_w. The acoustic properties of distilled water, i.e., the values of the velocity [28], attenuation coefficient [30], and density [37], are exactly known as a function of temperature, and they are found to be stable physically and chemically. It has also been reported that the effect on the velocity of dissolved air in water is negligible (less than 10 parts per million) at all temperatures [38]. The determination of the leaky wave velocity should be made using the velocity of water corresponding to the temperature at which the $V(z)$ curve measurements are performed. Dissolved air in the water may increase the propagation loss and slightly influence the attenuation measurement.

III. Line-Focus-Beam Acoustic Microscope System

A. Acoustic Line-Focus Beam

The acoustic line-focus beam employed here can be readily realized by constructing a sapphire acoustic lens

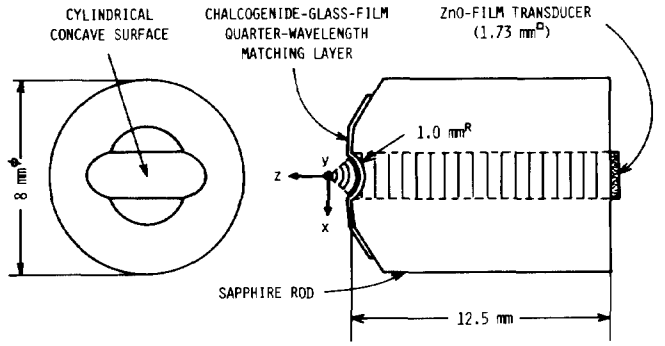

Fig. 8. Structure of acoustic line-focus-beam sapphire lens with cylindrical concave surface.

with a cylindrical concave surface. One example of the lens structure, including the dimensions, is depicted in Fig. 8. The cylindrical concave surface is formed with a curvature of 1.0 mm radius and an aperture half-angle of $\theta_M = 60°$ on one end of a Z-cut sapphire rod. The surface is polished to an optical finish. The dimensions and shape of the acoustic sapphire lens are designed to be suitable for $V(z)$-curve measurements at an operating frequency of about 200 MHz. The design criteria include the following four points:

1) effective use of acoustic field distribution in the Fresnel region of $l < a^2/\lambda$, where l is the distance between the transducer plane and the top surface of the lens, $2a$ is the transducer width, and λ is the wavelength in the sapphire rod;
2) sufficient translation distance for the $V(z)$-curve measurements without overlapping a signal that is reflected from a sample with the repeated echoes appearing at a period of $2l/v_s$, where v_s is the longitudinal velocity of sapphire (see Fig. 9);
3) suppression of spurious signals caused by the internal reflections in the sapphire rod; and,
4) acoustic attenuation of water through the propagation path.

On the cylindrical concave surface, a chalcogenide glass film with a thickness of a quarter wavelength is deposited, by vacuum-evaporation, as an acoustic antireflection coating for efficient transmission of acoustic waves across the sapphire–water interface [39]. On the flat surface of the lens, a ZnO-film transducer with dimensions 1.73×1.73 mm^2 is fabricated to radiate and detect longitudinal acoustic waves.

The performance of the acoustic line-focus-beam lens and transducer assembly was evaluated using an RF pulse of 0.4 μs in width at a frequency of 202 MHz, which corresponds to a quarter-wavelength frequency of the chalcogenide–glass–film acoustic matching layer. Before the experiments, a Z-cut sapphire reflector was placed on a precisely adjustable mechanical instrument and positioned at the focal point of the acoustic lens through a coupling liquid of water. Fig. 9 shows oscilloscope traces illustrating the performance of a typical lens and transducer assembly. Fig. 9(a) shows the receiving waveform

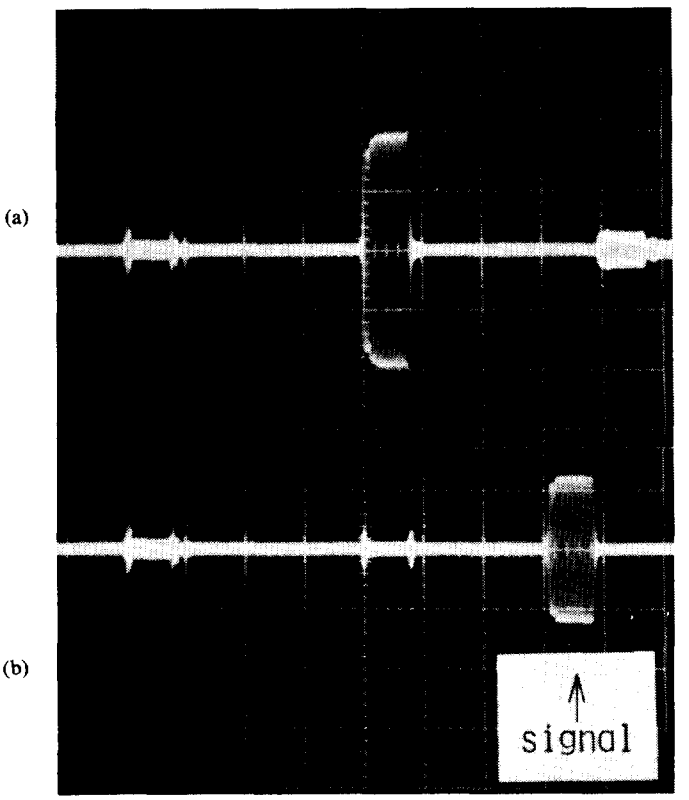

Fig. 9. Oscilloscope traces showing performance of acoustic line-focus-beam lens and transducer with RF pulse of 0.4 μs wide at 202 MHz. (a) Without water. (b) With water. Scales: vertical, 0.2 V/div, horizontal, 0.5 μs/div.

without water on the lens surface. The first pulse is a reflected pulse at the input electrical terminal of the transducer due to electrical impedance mismatching. The second and third echoes are acoustically reflected echoes from the top surface of the lens. Fig. 9(b) shows a receiving waveform when water coupling is introduced between the lens and the sapphire reflector positioned at the focal point. From the delayed time of the signal in the photograph, the focal length of this lens is measured as 1.14 mm by using the longitudinal velocity in water of $v_w = 1483$ m/s at 20°C. This value is in good agreement with the calculated value of 1.15 mm from the relation, $f_l = R/(1 - C)$, where $C = v_w/v_s$, and R is the radius of curvature. It is also seen that the second and third echoes are reduced due to the effect of the chalcogenide film antireflection coating. A system dynamic range of more than 40 dB is achieved in this way.

Further characterization of the acoustic field in water was carried out. Fig. 10 shows the experimental results of the acoustic field distributions along three axes, which are measured automatically by motor-driven translations. Figure 10(a) is the acoustic field distribution along the x axis. The three-decibel width is about 8 μm, which is comparable to an acoustic wavelength of 7.34 μm in water at a frequency of 202 MHz. Fig. 10(b) is the acoustic field distribution along the y axis. The intensity gives a maximum near the center ($y = 0$) and decreases with increasing distance $|y|$ as predicted by the theory of the

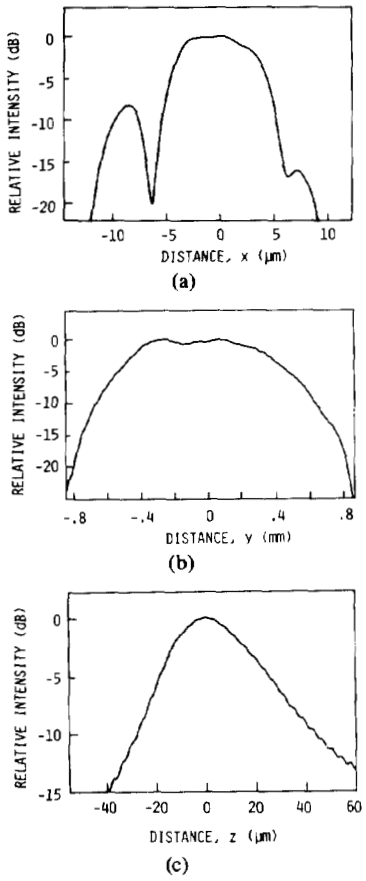

Fig. 10. Acoustic field distributions by acoustic line-focus-beam sapphire lens with cylindrical concave surface of 1.0 mm in radius measured at 202 MHz. (a) Along x axis. (b) Along y axis. (c) Along z axis.

acoustic field from the transducer with a finite electrode width [40]. Fig. 10(c) shows the acoustic field distribution along the z axis. The three-decibel width is about 32 μm, about four times larger than an acoustic wavelength. Thus it has been easily confirmed that, by employing the acoustic lens with a cylindrical concave surface, the acoustic plane waves radiated from the ZnO-film transducer are satisfactorily converted into an acoustic line-focus beam that is focused linearly along the y axis.

B. System

The normal configuration of the line-focus-beam acoustic microscope for material characterization is shown in Fig. 11. The system consists of four main elements; viz., the acoustic probe, pulse-mode measurement system for transmitting and receiving electrical signals, mechanical alignments and movements to record $V(z)$ curves, and a computer for controlling the system and processing the recorded waveforms.

An RF pulse from the pulse-mode measurement system [41], which is fundamentally composed of a spectrum analyzer and tracking generator, excites a ZnO-film transducer in the acoustic microscope, and pulsed acoustic plane waves are propagated in the lens rod. Typically, the pulse width is 0.5 μsec for the line-focus-beam lens described in the previous section, and the repetition frequency is 10 kHz. The transducer also acts as a receiver and picks up all reflected pulses. The reflected pulses are fed into the pulse mode measurement system through a circulator. An RF gate circuit with a high on-off ratio is used to extract the signal reflected from a sample, which carries the acoustic information from all other reflected pulses. Care is taken to position a gate pulse of the correct width because the delay time of a reflected signal from the sample varies with the position of the sample. The pulsed video output that results from the detection of the RF pulse signal is converted into a conventional video output, which is also the acoustic microscope output, using a peak-holding circuit.

The sample is placed on a mechanical stage for upward and downward movement along the beam axis. The transducer output detected with the line-focus beam is very sensitive to alignment between sample and lens because the acoustic field is much wider in the y-axis direction than an acoustic wavelength. For precise measurements, the sample and the assembly of the acoustic lens and transducer should be mounted on a mechanical stage that is movable along x, y, and z axes and rotatable around these axes with very high accuracy. The sample is positioned at the focal point of the lens. The transducer output for a signal reflected from the sample is maximized with careful alignment. The translation along the z axis is driven by a stepping-motor for which one step corresponds to a distance of 0.1 μm.

$V(z)$ curves are recorded in the memory of a digital wave analyzer, synchronized with the driving signal to the stepping-motor and then entered into a computer. The useful axial range for the lens described in the last section is 550 μm.

In the present measurement setup, a coupling liquid of distilled water is employed as an essential reference medium. Experiments are performed, recording the temperature of water and the acoustic frequency. Using a set of these data (the $V(z)$ curve, temperature, and acoustic frequency), the determination of acoustic properties of phase velocity and attenuation of leaky waves is made according to the processing procedure as described in detail in the next section.

C. Processing Procedure of $V(z)$ Curves

On the basis of the measurement principle proposed in Section II, we apply an FFT waveform analysis to determine the acoustic properties we require from $V(z)$ curves.

A flowchart of the fundamental processing procedure is shown in Fig. 12. Several schematic waveforms at key points in the process are depicted in Fig. 13. The $V(z)$ data are recorded initially on a logarithmic scale (Fig. 12(a)). It is then converted into a linear scale (Fig. 12(b)), where a $V(z)$ curve for Pb, which is measured under the same experimental conditions as the $V(z)$ curve to be analyzed, is used as an approximated $V_L(z)$ and denoted here as $V_L'(z)$. We obtain a $V_I'(z)$ curve by subtracting the $V_L'(z)$ from the $V(z)$ (Fig. 12(c)). Then we use digital low-pass filtering techniques (for example, moving average)

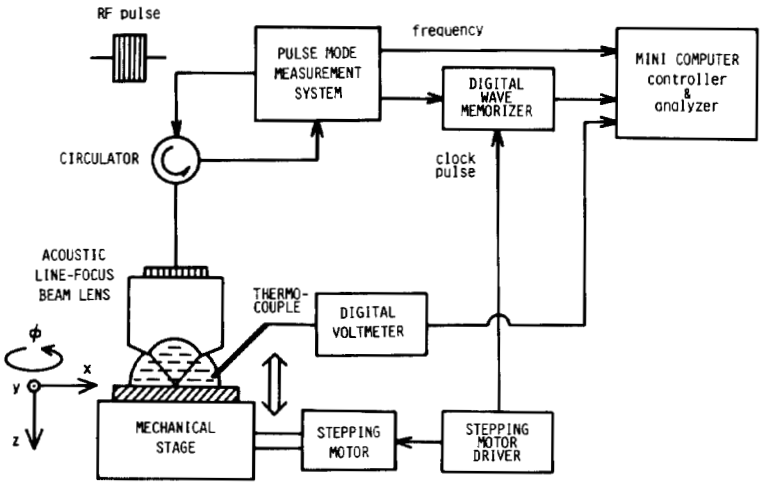

Fig. 11. Block diagram of the line-focus-beam acoustic microscope system.

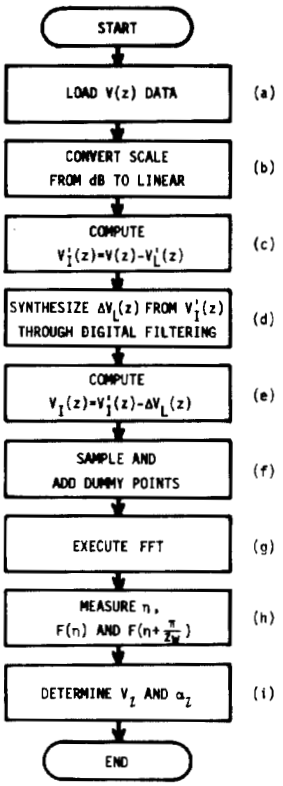

Fig. 12. Flow chart of processing procedure for $V(z)$ curve analysis.

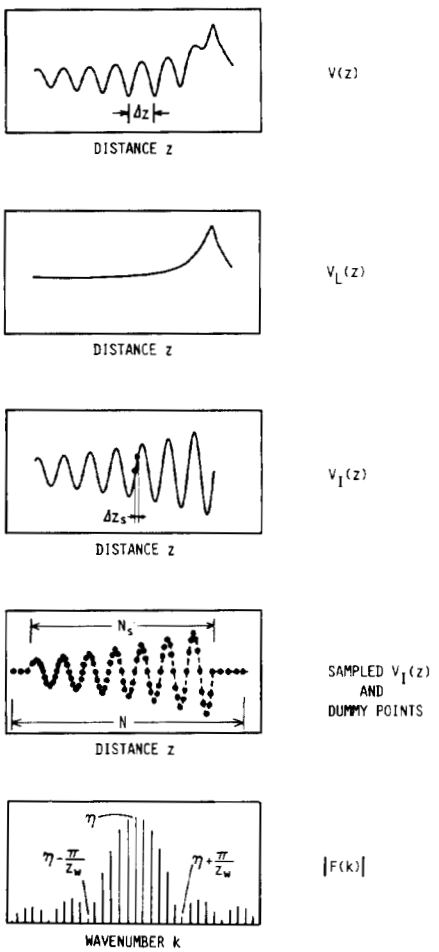

Fig. 13. Schematic waveforms at key points in $V(z)$ curve analysis.

to attenuate frequency components higher than those corresponding to the interference periodicity, and synthesize a $\Delta V_L(z)$ curve (Fig. 12(d)). Further, by subtracting the $\Delta V_L(z)$ from the $V_I'(z)$, we can extract the fine $V_I(z)$ to be analyzed (Fig. 12(e)). The $V_L(z)$ defined in (5) is formed here by summing $V_L'(z) + \Delta V_L(z)$, which is derived by the techniques just mentioned. This processing is most important to obtain a sufficient measurement accuracy for material characterization.

Next we sample the measured $V_I(z)$ curves with the distance interval Δz_s. Sampling points N_s are distributed for the waveform in the characterization region. In making the analysis, we provide an additional N_d dummy sampling points both in front of and behind the $V_I(z)$ curves (Fig. 12(f)) in order to obtain a sufficiently high frequency resolution, which is directly related to the velocity resolution in the present method. So, a total of N points, where $N = N_d + N_s$, are used in the analysis. The frequency interval Δk in the frequency domain is given

by

$$\Delta k = 2\pi/(N \cdot \Delta z_s). \quad (31)$$

Applying the FFT analysis to the waveform (Fig. 12(g)), we obtain a spectral distribution as shown in Fig. 13(e). From the distribution, we have a center frequency η giving a maximum spectrum, corresponding to the characteristic dip interval Δz. We also determine in the distribution two specified spectra of $F(\eta)$ and $F(\eta + \pi/z_w)$ (Fig. 12(h)).

Using the water temperature T recorded at the same time as the $V(z)$ curve measurement was made, the acoustic property of water $v_w(T)$ and $\alpha_w(T)$, which is required for the determination of the final characteristics of the leaky wave on the water-sample boundary, is calculated by the computer. With the dip interval Δz obtained by the FFT analysis using (15), we can determine the velocity v_l. Using (28), (29), and (12) with the two spectra, we can also determine the attenuation factor α_l (Fig. 12(i)).

In the processing of highly deformed $V(z)$ curves due to the multimode interference mechanism, we firstly search for the number of leaky wave modes and the rough mode spectra by applying an FFT analysis to the $V(z)$ curves. According to the procedures (d)–(i) in Fig. 12, the analysis is repeated for the $V_{In}(z)$ in each of the higher frequency modes to be analyzed, so that pairs of $v_l(n)$ and $\alpha_l(n)$ can be determined in turn.

In the present FFT analysis, we take a total of 8192 points (N), a sampling rate m of 15 $\sim$ 30 points per wavelength and the ratio $N/N_s = 30 \sim 50$, depending on the acoustic properties of the materials being studied. Further, in the analysis we use an interpolation to measure the two specified spectra properly. In this way the acoustic properties can be determined without the errors caused by the discrete spectra distributed in the frequency domain. Details of the FFT analysis and setting of the parameters for the analysis will be published elsewhere.

IV. Experiments

Experimental determination of acoustic properties for materials by the line-focus-beam acoustic microscope is carried out at a frequency of 225 MHz in order to verify the validity of the method described in Section II. Experimental results are compared with theoretical results calculated by the analytic procedure of Campbell and Jones [42] for analyzing the propagation characteristics of leaky waves on the water–solid boundary. Several materials—including Y-cut α-quartz, (111) Ge, and isotropic substrates such as tellurite glass and borosilicate glasses—and polymer samples are examined for the demonstration. The system is further applied to a variety of materials; for example, single crystals with special crystalline planes, some typical samples of layered SiO_2-film/Z-cut sapphire, and a membrane structure of thin borosilicate-glass film. All the leaky wave modes associated with the interference phenomena in $V(z)$ curves, such as leaky SAW, leaky pseudo-SAW, leaky SSCW, leaky Lamb wave, and harmonic waves, are investigated.

A. Semi-Infinite Sample

1) Leaky SAW: We first applied the system to measure the acoustic properties of a piezoelectric Y-cut α-quartz plate with an optically polished surface. Fig. 14(a) shows the $V(z)$ curve measured for the z-axis propagation direction ($\phi = 90°$ in Fig. 15) of the LSAW mode on the water–Y-cut α-quartz boundary. In the negative z region, where material characterization is possible, the curve varies markedly with the distance z, and the dips in the curve appear periodically, while the amplitude of interference attenuates rapidly with decreasing distance z. Fig. 14(b) is the $V(z)$ curve for polycrystalline lead. According to the measurement procedure, the $V_I(z)$ for the α-quartz (shown in Fig. 14(c)) can be extracted by employing the $V(z)$ curve for lead as the characteristic lens response $V_L(z)$. From the $V_I(z)$, we can determine directly that the velocity of leaky SAW is 3820 m/s with a dip interval of $\Delta z = 41.81$ μm. From the envelope of $V_I(z)$ decreasing at the rate of 69 dB/mm in Fig. 14(d), we can also determine the normalized attenuation factor of 3.36×10^{-2} and substitute the relevant values into (11) and (12).

Experimental results are in good agreement with the values of $v_{\mathrm{LSAW}} = 3826$ m/s and $\alpha_{\mathrm{LSAW}} = 3.47 \times 10^{-2}$ calculated by using the physical constants for α-quartz reported in [43] and for water a longitudinal velocity of $v_w = 1483$ m/s and a density $\rho = 998.2$ kg/m^3 at 20°C. The differences are about 0.14 percent in velocity and about 2.7 percent in attenuation as shown in Table I.

In Fig. 14(e) the distribution of spectra analyzed by an FFT for the $V_I(z)$ in Fig. 14(c) is shown. A one mode spectrum for a leaky SAW appears clearly at a frequency of $k = 0.1503$ rad/μm. Using (30) and (15), the velocity can be calculated as $v_{\mathrm{LSAW}} = 3820$ m/s. From two spectra in the distribution at $k = 0.1503$ and 0.1634, we can determine the attenuation in (28). Finally, the normalized attenuation factor α_{LSAW} on the boundary is calculated to be 3.36×10^{-2} using (29) and (12). Both values are naturally in excellent agreement with those determined above by the direct method.

In this demonstration the attenuation can be largely attributed to the water loading effect on the substrate, which results from the following.

1) The scattering attenuation factor α_s in (13) due to surface roughness, grain boundaries, internal defects, etc., is considered to be negligible.
2) The bulk absorption attenuation factor α_b mainly caused by the viscous effect is theoretically estimated to be negligibly small compared with the attenuation factor α_{LSAW} due to the acoustic water loading effect [44], because the attenuation coefficients for α-quartz are much smaller than those for fused quartz [45].

For the velocity, the water loading effect gives rise to a calculated velocity for the leaky SAW that is 15 m/s larger

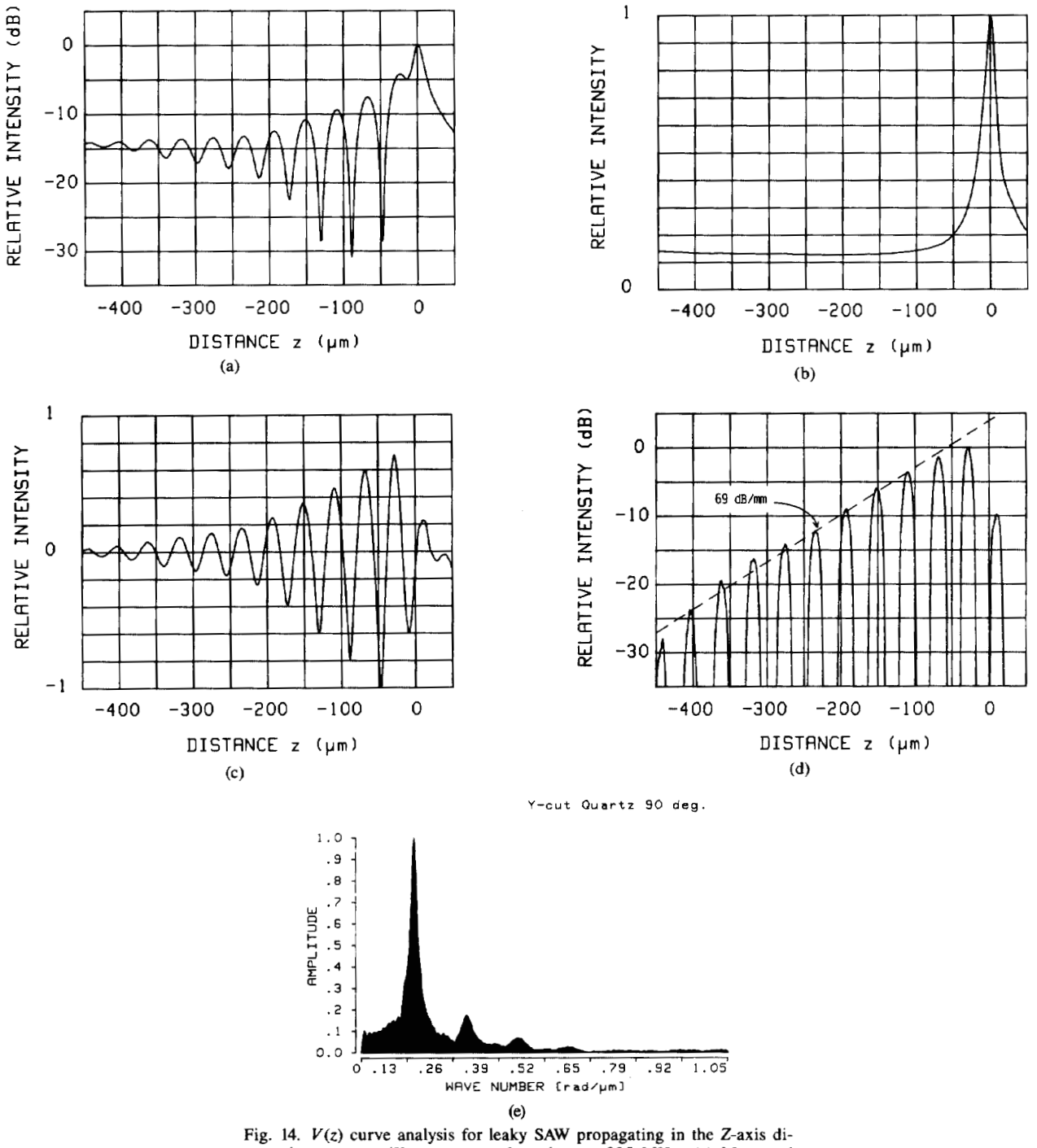

Fig. 14. $V(z)$ curve analysis for leaky SAW propagating in the Z-axis direction on water/Y-cut-α-quartz boundary at 225 MHz. (a) Measured $V(z)$. (b) Measured $V_L'(z)$ of Pb. (c) $V_1(z)$. (d) $\log(V_1(z))$. (e) $|F(k)|$.

than that of 3811 m/s for a SAW propagating along the same direction on a free surface of α-quartz.

In the same way the propagation characteristics of a leaky SAW is measured for other propagation directions using the FFT method. The experimental results are plotted as open circles in Fig. 15 together with the theoretical results as the solid line. The variation of leaky SAW velocities measured extends from 3165 m/s ($\phi = 0°$) with the normalized attenuation factor of 2.57×10^{-2} to 3820 m/s ($\phi = 90°$) with 3.38×10^{-2}. The calculated phase velocities range from 3171 m/s ($\phi = 0°$) with 2.48×10^{-2} to 3826 m/s ($\phi = 90°$) with 3.47×10^{-2}. The measured values are as a whole very close to the calculated values within the differences of about 0.2 percent in velocity and about four percent in attenuation.

Thus, it has been demonstrated that using this method the acoustic system can detect precisely the propagation characteristics, including anisotropy, of Y-cut α-quartz for the leaky SAW mode as a function of the wave propagation directions around the Y axis.

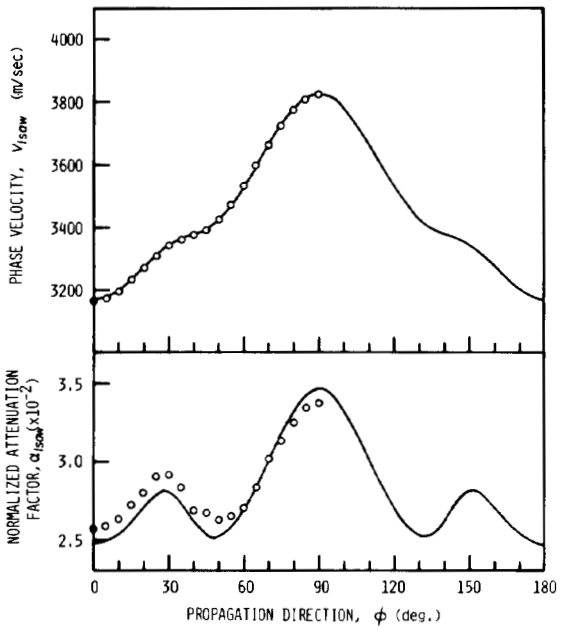

Fig. 15. Experimental and calculated results of propagation characteristics of leaky SAW's on water/Y-cut-α-quartz boundary. ○ denotes measured, and —— denotes calculated.

TABLE I
COMPARISON OF EXPERIMENTAL RESULTS WITH CALCULATED RESULTS OF PROPAGATION CHARACTERISTICS FOR LEAKY SAW IN THE Z-AXIS DIRECTION ON WATER-Y-CUT α-QUARTZ BOUNDARY

Phase velocity v_{LSAW} (m/s)		Normalized attenuation factor α_{LSAW}	
Measured	Calculated	Measured	Calculated
3820	3826	3.36×10^{-2}	3.47×10^{-2}

2) Leaky Pseudo-SAW: The measurement method has been further applied to the determination of acoustic properties for a sample of (111) Ge, where one more leaky pseudo-SAW mode actively participates in the interference phenomena of the $V(z)$ curves. The leaky pseudo-SAW is named here for a wave derived from the water loading for the pseudo-SAW propagating on the free surface of the germanium. The leaky pseudo-SAW propagates on the water–sample boundary, reradiating the acoustic energy of the wave into both water and the substrate. Germanium belongs to the m3m crystal class. Propagation characteristics of the two leaky waves on water–(111)-Ge boundary are determined completely from the analysis for the wave propagation directions in the range between $\phi = 0°$ and 30° because of the crystalline symmetry. Both waves exist theoretically in all directions except the equivalent direction of $\phi = 30°$ for pure Rayleigh mode.

The $V(z)$ curves measured for two typical directions of $\phi = 0°$ and 30° are shown in Fig. 16(a) and (b), respectively. In the case of the $V(z)$ curve for $\phi = 0°$, shown in Fig. 16(a), the curve has apparently complex and deformed variation both in dip intervals and in shape in the

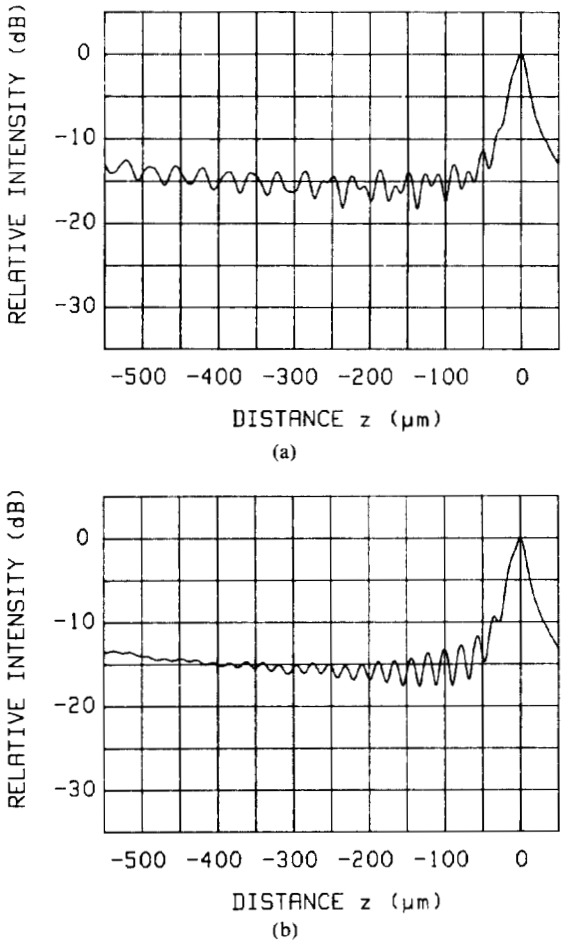

Fig. 16. $V(z)$ curves on water–(111)-Ge boundary measured at 225 MHz. (a) $\phi = 0°$ ([110]). (b) $\phi = 30°$ ([112]).

characterization region because of the multimode interference. As stated in an earlier discussion of the multimode interference mechanism, the curve should be decomposed into two elemental $V_l(z)$ curves with the respective acoustic properties of leaky SAW and pseudo-SAW modes, as presented in Table II. In a region between $z = 0$ and -300 μm, the curve is significantly deformed because two elemental $V_l(z)$ curves have almost the same amplitude but different periodicity of dips. While in a region between -300 and -550 μm, the amplitude of an elemental curve for the leaky pseudo-SAW is much larger than that for the leaky SAW so that the corresponding dip periodicity appears dominantly. On the other hand, in the case of the $V(z)$ curve for $\phi = 30°$ shown in Fig. 16(b), the interference is observed with a constant interval of dips and simple variation in shape of the $V(z)$ curve because only a leaky pure Rayleigh wave can propagate in this direction on the boundary.

Now we apply the FFT analysis to the $V(z)$ curves. Figure 17(a) and (b) show the results for the two $V(z)$ curves of Fig. 16(a) and (b), respectively. In Fig. 17(a) two mode spectra for a leaky SAW and a leaky pseudo-SAW appear clearly with moderate spectral distributions at frequencies of k_p (LSAW) = 0.3229 and k_p (LPSAW) = 0.1874, respectively. Values of $v_{LSAW} = 2675$ m/s and $\alpha_{LSAW} =$

TABLE II
COMPARISON OF EXPERIMENTAL RESULTS AND CALCULATED RESULTS FOR (111) Ge

Propagation direction ϕ	Leaky SAW				Leaky pseudo-SAW			
	Velocity v_{LSAW} (m/s)		Normalized attenuation factor α_{LSAW}		Velocity v_{LPSAW} (m/s)		Normalized attenuation factor α_{LPSAW}	
	Measured	Calculated	Measured	Calculated	Measured	Calculated	Measured	Calculated
0°	2675	2691	1.14×10^{-2}	1.11×10^{-2}	3444	3450	0.49×10^{-2}	0.53×10^{-2}
30°	2813	2828	1.57×10^{-2}	1.55×10^{-2}	—	—	—	—

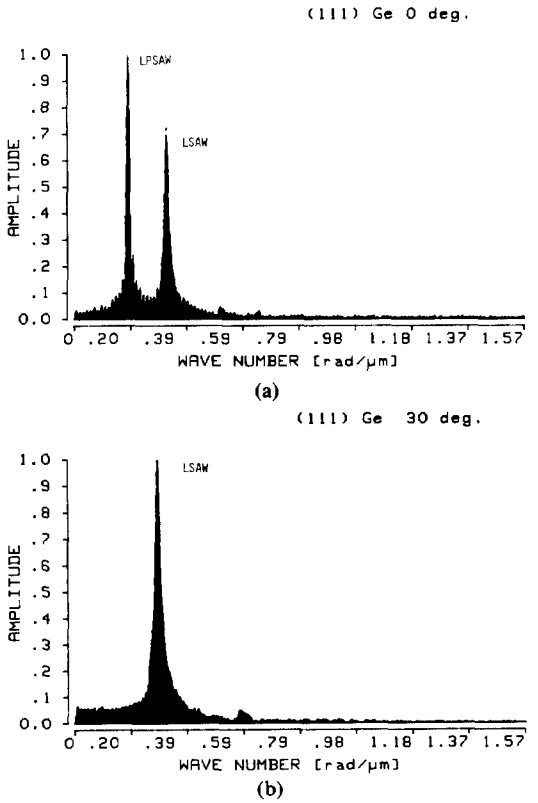

Fig. 17 FFT-analyzed mode spectra for $V(z)$ curves shown in Fig. 16. (a) $\phi = 0°$. (b) $\phi = 30°$.

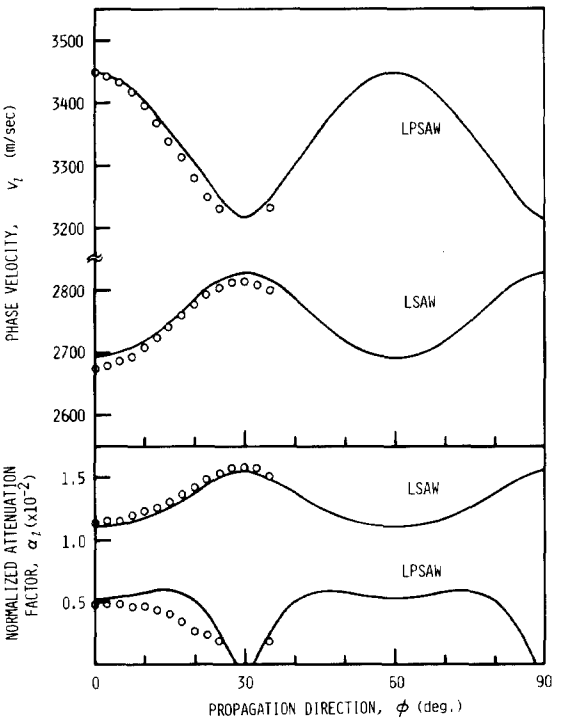

Fig. 18. Experimental and calculated results of propagation characteristics of leaky SAW and leaky pseudo-SAW on water–(111)-Ge boundary. A leaky pseudo-SAW mode does not exist at $\phi = 30°$. o denotes measured, and —— denotes calculated.

1.14×10^{-2} are determined for the leaky SAW mode and those of $v_{LPSAW} = 3444$ m/s and $\alpha_{LPSAW} = 0.49 \times 10^{-2}$ for the leaky pseudo-SAW. These values are very close to the calculated values, as shown in Table II. In Fig. 17(b), only one significant mode spectrum is measured for a leaky pure Rayleigh wave mode, with a center frequency of k_p (LSAW) = 0.2890. The velocity is calculated to be $v_{LSAW} = 2813$ m/s, and the attenuation is $\alpha_{LSAW} = 1.57 \times 10^{-2}$.

Fig. 18 shows the results measured for the other propagation directions in the same way together with the theoretical results drawn by the solid line. In the calculations the physical constants in [46] are used for germanium. It is easily seen that an accurate determination of the acoustic quantities has been possible for each mode existing on the boundary. The differences between the measured and calculated results are within 0.6 percent for the velocity of both modes, a few percent for the attenuation of the leaky SAW mode, and more than seven percent for the leaky pseudo-SAW mode. The difference in the attenuation for the leaky pseudo-SAW becomes greater as the propagation direction approaches near $\phi = 30°$. This is due to the low level excitation efficiency of the leaky pseudo-SAW on the boundary. The problem of the attenuation measurement accuracy will be examined in Section V-B.

3) Leaky SSCW: On the water–semi-infinite-sample boundary yet another leaky wave mode, the leaky SSCW mode, can be excited efficiently as the third mode available for the material characterization where the longitudinal wave velocity of the sample is relatively small. Experiments are performed for some polymer samples of polymethylmethacrylate (PMMA), polyvinyl chloride (PVC), and polystyrene; and some kinds of glasses, such as tellurite glass, fused quartz (SiO_2), borosilicate glasses of E6 (Ohara Optical Glass Manufacturing Company, Ltd.), and Pyrex (Corning Company, Ltd., no. 7740).

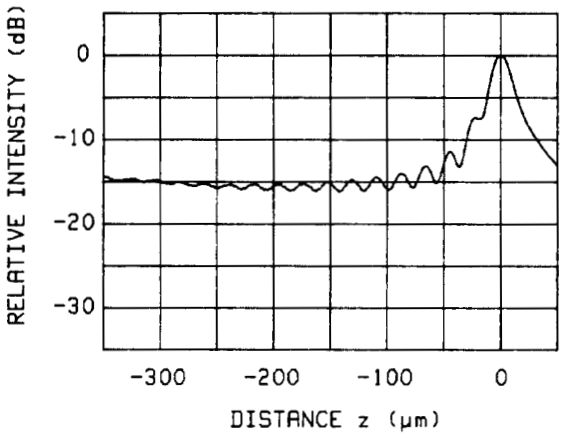

Fig. 19. $V(z)$ curves on water/PMMA boundary measured at 225 MHz.

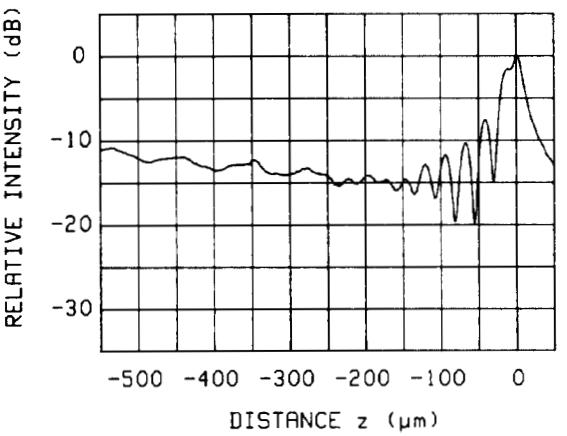

Fig. 20. $V(z)$ curves on water/E6-glass boundary measured at 225 MHz.

TABLE III
COMPARISON OF EXPERIMENTAL RESULTS WITH CALCULATED RESULTS FOR SOME TYPICAL ISOTROPIC SAMPLES

	Leaky SAW				Leaky SSCW		
	Velocity v_{LSAW} (m/s)		Normalized attenuation factor α_{LSAW} (m/s)		Velocity v_{LSSCW} (m/s)		Normalized attenuation factor α_{LSSCW}
Sample	Measured	Calculated	Measured	Calculated	Measured	Calculated	Measured
PMMA	—	—	—	—	2787	2730[1]	2.19×10^{-2}
PVC	—	—	—	—	2365	2240[1]	2.21×10^{-2}
Polystyrene	—	—	—	—	2322	2340[1]	2.22×10^{-2}
Tellurite glass [56]	—	1817	—	3.64×10^{-2}	3446	3460	1.27×10^{-2}
SiO_2 [48]	3415	3430	3.90×10^{-2}	3.82×10^{-2}	5870	5980	1.38×10^{-2}
7740[2]	3132	3140	4.27×10^{-2}	4.03×10^{-2}	5470	5608	1.57×10^{-2}
E6[3]	3042	3041	4.60×10^{-2}	4.33×10^{-2}	5350	5401	1.43×10^{-2}

[1]A typical longitudinal velocity.
[2]Technical data from Corning Co. Ltd.
[3]Technical data from Ohara Optical Mfg. Co. Ltd.

Fig. 19 shows the $V(z)$ curve observed for the PMMA. There is a regular interference pattern for only one mode of leaky SSCW having a velocity of $v_{LSSCW} = 2787$ m/s and an attenuation of $\alpha_{LSSCW} = 2.19 \times 10^{-2}$. Fig. 20 shows the $V(z)$ curve for E6 glass. There, we can see clearly the leaky SSCW ($\Delta z = 84.15$ μm) in the $V(z)$ curve in addition to the leaky Rayleigh wave with a dip interval of $\Delta z = 25.98$ μm. For the glasses, the acoustic quantities for leaky SSCW's as well as leaky Rayleigh waves are determined, as shown in Table III. The measured values for leaky SAW's are very close to the calculated values, while for leaky SSCW's there are slight differences of a few percent between them. In Table III the longitudinal velocities for polymer samples are also given for reference. The acoustic properties of leaky SSCW's propagating on the boundary are measured properly by the acoustic microscope system.

B. Layered Sample (Harmonics)

In this section experiments are described concerning the determination of acoustic properties for leaky waves propagating on samples of SiO_2 film Z-cut sapphire as an example of a layered structure. SiO_2 films were fabricated on the substrates by planar magnetron RF sputtering, for several film thicknesses. Sputtering conditions were as follows: a gas mixture of Ar (80 percent) and O_2 (20 percent) at a pressure of 4×10^{-3} Torr, a substrate temperature of 200°C, and a deposition rate of 1.5 μm. The film thickness was determined by observing the interference patterns of a He–Ne laser beam during sputtering.

The measurements were made on the y-axis propagation direction of Z-cut sapphire where a leaky pure Rayleigh wave can propagate as a fundamental mode. Fig. 21 shows the $V(z)$ curves measured for four typical samples with film thicknesses of 0, 2.170, 5.426, and 10.852 μm. From the $V(z)$ curve for a naked sapphire substrate, we can extract only a leaky Rayleigh wave with a velocity of 5710 m/s and an attenuation of 0.89×10^{-2}, corresponding to the theoretical values of 5711 m/s and 0.92×10^{-2}, respectively. By depositing SiO_2 films, the curves vary markedly in form. In the case of the SiO_2 film of 2.170 μm in thickness (Fig. 21(b)), the velocity of $v_{LSAW} = 5483$ m/s and the attenuation of $\alpha_{LSAW} = 1.19 \times 10^{-2}$ are determined for the leaky pure Rayleigh wave. In the case of the film of 5.426 μm (Fig. 21(c)), it is easily seen that an additional leaky wave mode participates in the interference of the $V(z)$ curve as similarly

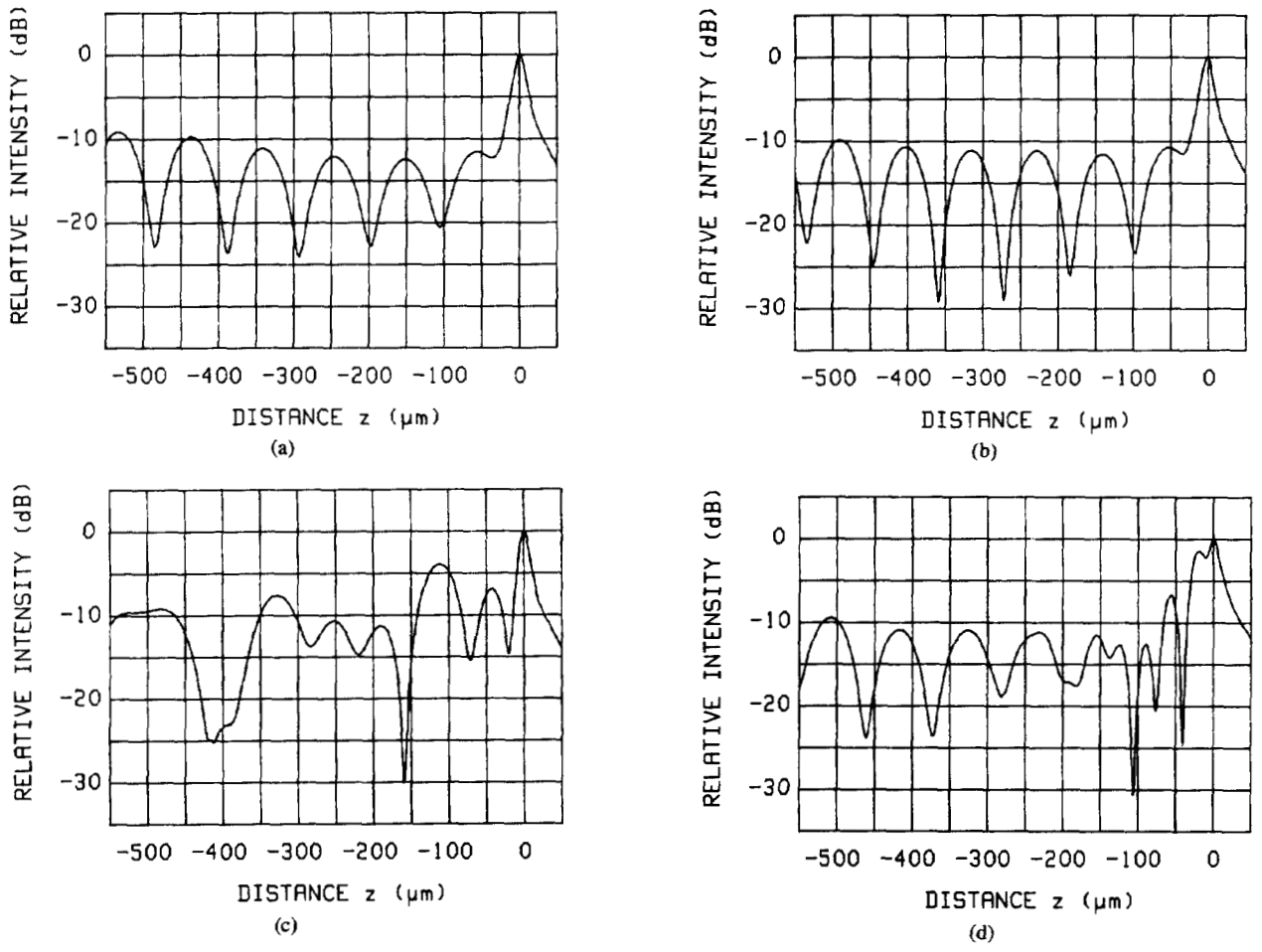

Fig. 21. $V(z)$ curves on water/SiO_2-film/Z-cut-sapphire measured at 225 MHz. (a) $H = 0$. (b) $H = 2.170$ μm. (c) $H = 5.426$ μm. (d) $H = 10.852$ μm.

TABLE IV
COMPARISON OF EXPERIMENTAL RESULTS WITH CALCULATED RESULTS FOR SiO_2-FILM/Z-CUT SAPPHIRE

Film thickness (μm)	Leaky SAW				Other leaky waves			
	Velocity v_{LSAW} (m/s)		Normalized attenuation factor α_{LSAW}		Velocity v_l (m/s)		Normalized attenuation factor α_l	
	Measured	Calculated	Measured	Calculated	Measured	Calculated	Measured	Calculated
0	5710	5711	0.89×10^{-2}	0.92×10^{-2}	—	—	—	—
2.170	5483	5477	1.19×10^{-2}	1.24×10^{-2}	—	—	—	—
5.426	4957	4958	5.07×10^{-2}	4.56×10^{-2}	8435[1]	8335	—	3.83×10^{-2}
10.852	3443	3562	5.39×10^{-2}	5.43×10^{-2}	5574[2]	5662	0.28×10^{-2}	0.63×10^{-2}

[1]Leaky pseudo-SAW mode.
[2]Harmonic mode of leaky SAW.

observed for the (111) Ge. For a leaky Rayleigh wave, a velocity of $v_{LSAW} = 4957$ m/s and an attenuation of $\alpha_{LSAW} = 5.07 \times 10^{-2}$ are determined, and they coincide with the calculated values of $v_{LSAW} = 4958$ m/s and $\alpha_{LSAW} = 4.56 \times 10^{-2}$. Another mode is a leaky pseudo-Rayleigh wave with a velocity of $v_{LPSAW} = 8435$ m/s, corresponding to a calculated value of $v_{LPSAW} = 8335$ m/s. In the case of the film of 10.852 μm, we can clearly measure two leaky modes; one is a fundamental leaky Rayleigh wave with $v_{LSAW} = 3443$ m/s and $\alpha_{LSAW} = 5.39 \times 10^{-2}$; and another is a harmonic mode of the leaky Rayleigh wave with $v_{LSAW} = 5574$ m/s and $\alpha_{LSAW} = 0.28 \times 10^{-2}$. The measured values of acoustic properties agree well with the calculated values as shown in Table IV. Experimental results are shown against the normalized parameter of fH (the product of the acoustic frequency and the film thickness) in Fig. 22 together with the calculated results. In the calculations the physical constants for sapphire reported in [47] and for SiO_2 in [48] are used, respectively.

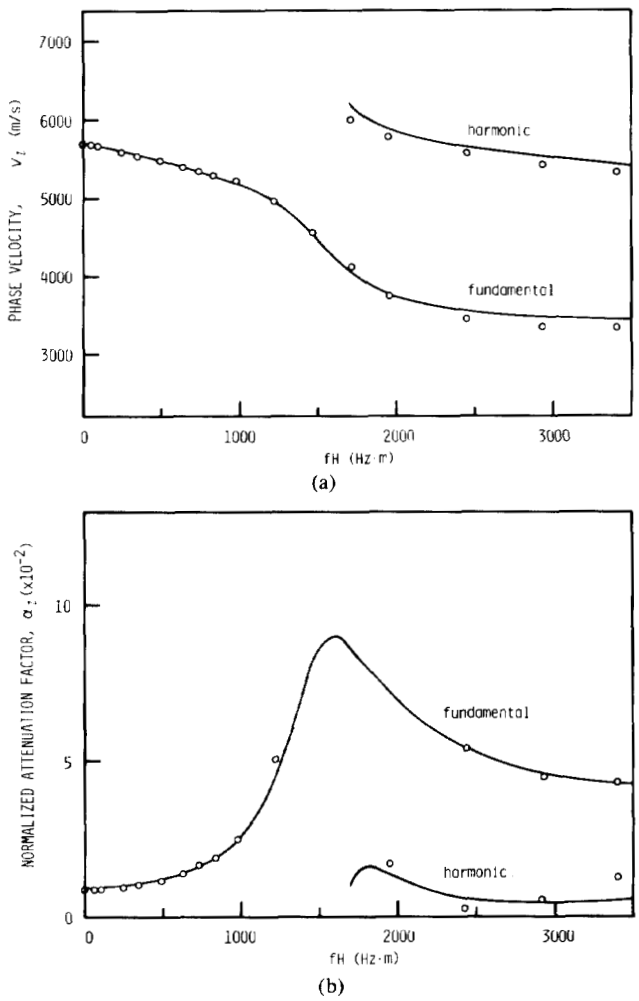

Fig. 22. Experimental and calculated results of propagation characteristics of leaky SAW on water/SiO_2 film/Z-cut sapphire. ○ denotes measured, and —— denotes calculated. (a) Velocity. (b) Attenuation.

The measurements show clearly that the propagation characteristics for both the velocity and attenuation of related leaky waves are dispersive depending greatly on the value of *fH*. The good agreement shows us that the SiO_2 films prepared here have almost the same acoustic properties as those of bulk SiO_2. It suggests that the line-focus-beam acoustic microscope system is available for determining the physical constants, such as the elastic constants and the density, for films through the theoretical calculations using the measured acoustic properties for the films and substrates, after the naked substrates are completely characterized.

C. Thin-Film Sample (Leaky Lamb Wave)

The remaining mode to be measured by the present acoustic system is a leaky Lamb wave. The wave exists on thin-film samples where there is water loading on one or both sides. Here measurements are made of an optically polished borosilicate glass (Tempax glass is manufactured commercially by Schott Company, Ltd.) of 24 μm in thickness, with water loaded on only one side of the sample. Measurements are performed by varying the frequency in 5-MHz increments from 50 MHz to 100 MHz,

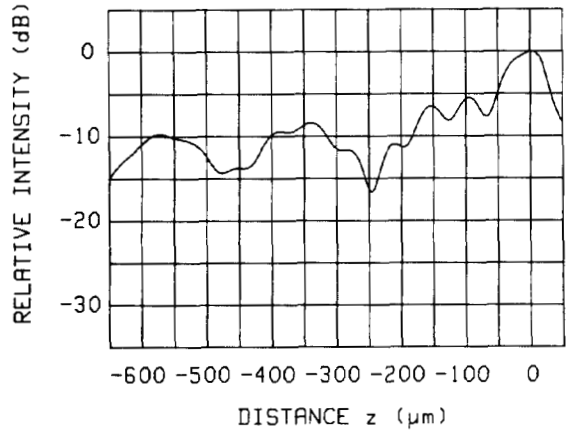

Fig. 23. $V(z)$ curves on water/Tempax-glass-film/free-space measured at 85 MHz.

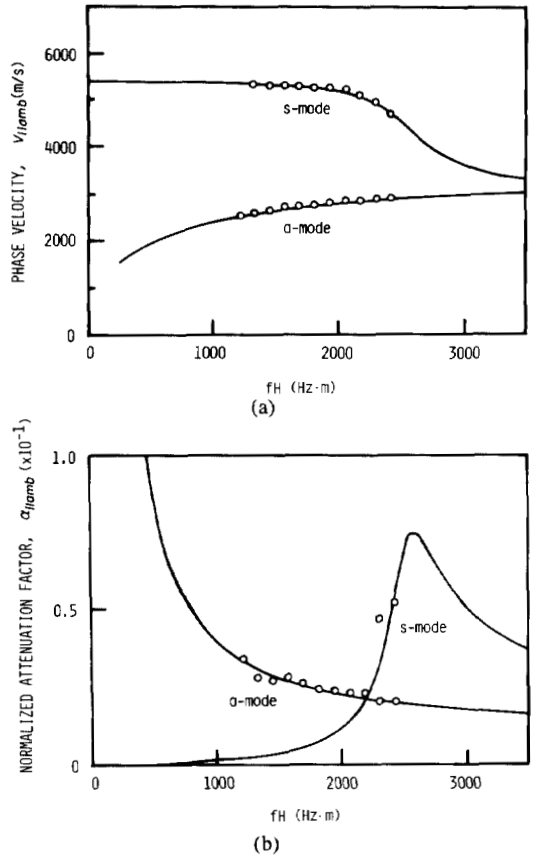

Fig. 24. Experimental and calculated results of propagation characteristics of leaky Lamb wave on water/Tempax-glass-film/free-space. The ○ denotes measured, and the —— denotes calculated. (a) Velocity. (b) Attenuation.

using an acoustic line-focus-beam sapphire lens of 1.5 mm in radius of curvature.

A typical $V(z)$ curve measured at 85 MHz is shown in Fig. 23. Two pairs of acoustic quantities corresponding to two modes can be determined from the curve: one has a velocity of $v_l = 2861$ m/s and an attenuation of $\alpha_l = 2.30 \times 10^{-2}$, and the other has a velocity of $v_l = 5227$ m/s. Analyzing the propagation characteristics of the fundamental waves for the structure of water–tempax-glass–free-space, there are two fundamental leaky Lamb waves of symmetric (*s*-mode) and antisymmetric (*a*-mode)

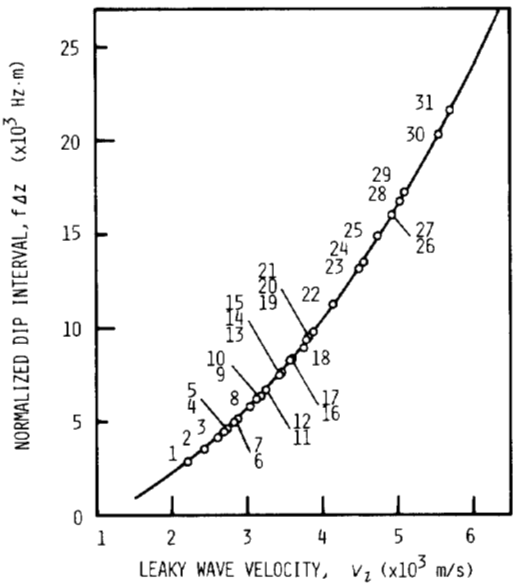

Fig. 25. Experimental results and theoretical calculations of material characterization curve. The —— denotes the experimental curve, and the ○ denotes the following theoretical values: 1) (111) InSb[a](LPSAW); 2) (111) GaAs[a]; 3) (111) GaAs[b]; 4) (111) Ge[a]; 5) (001) GaAs[c]; 6) (111) Ge[b]; 7) (001) GaAs[d]; 8) E6; 9) 7740; 10) *YX* α-Quartz; 11) (111) GaAs[a] (LPSAW); 12) (111) GGG[b]; 13) SiO_2; 14) (111) Ge[a] (LPSAW); 15) *YZ* $LiNbO_3$; 16) (001) YIG[d]; 17) (111) YIG[b]; 18) *YX* $LiNbO_3$; 19) *ZX* $LiNbO_3$; 20) *YZ* α-Quartz; 21) *ZY* $LiNbO_3$; 22) *XY* rutile; 23) (110) Si[f]; 24) (111) Si[a]; 25) (111) Si[b]; 26) *XZ* rutile; 27) (001) Si[c]; 28) (110) Si[e]; 29) (001) Si[d]; 30) *ZX* sapphire; and 31) *ZY* sapphire. *a*;[110], *b*;[112], *c*;[010], *d*;[110], *e*;[001], *f*;[110].

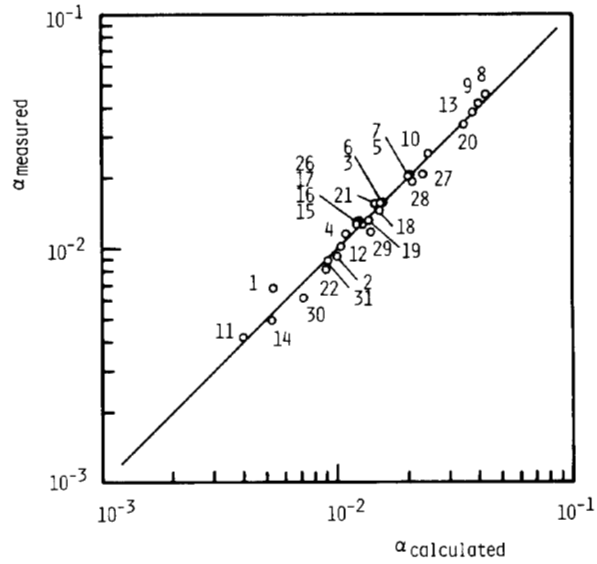

Fig. 26. Comparison of experimental results with theoretical results of normalized attenuation factor for materials shown in Fig. 25.

modes. The theoretical curves for both modes are shown in Fig. 24 with the physical constants of $C_{11} = 7.05 \times 10^{10}$ N/m^2, $C_{12} = 1.99 \times 10^{10}$ N/m^2, and $\rho = 2.23 \times 10^3$ kg/m^3. The calculated values compare well with the experimental results. The antisymmetric modes have low velocities (around 2800 m/s) and moderate attenuation factors so that the determination is made with ease, as compared with the case for the symmetric modes in the experimental region.

D. Material Characterization Curve

Here the acoustic microscope system is applied to a variety of solid materials, such as InSb, GaAs, YIG, GGG, Si, TiO_2, $LiNbO_3$, sintered SiC, diamond, etc., for which the velocities of leaky waves range widely from 2000 to 11000 m/s. The experimental results for all samples are compared with calculated values using their physical constants [49].

For the velocity measurements associated with leaky waves on the boundary of water–samples, we can develop the following normalized relation to obtain a universal representation for the material characterization

$$f\Delta z = v_w/2(1 - \cos\theta_l). \tag{32}$$

It is recognized that the product of $f\Delta z$ depends entirely upon the acoustic properties of materials and the reference liquid of water.

All the experimental results are seen to fall on a single experimental curve drawn by using (32). This curve is shown by the solid line in Fig. 25, and we call it the material characterization curve. In this figure the theoretical velocity values of leaky waves in the typical propagation directions for all the characterized materials are plotted as open circles for leaky SAW's and leaky pseudo-SAW's. It is apparent from the comparison that the material characterization curve determined by the measurements is well predicted by the theoretical values. The differences between the experimental and theoretical values are much less than 0.5 percent. As illustrated in Fig. 25, there is only one exceptionally excessive difference (1.2 percent for *X*-propagating on *Y*-cut $LiNbO_3$ (no. 18)), which has been shown to be due to the fact that the physical constants [50] used here are slightly different from those for the lithium niobate actually employed [19]. It is also confirmed that the system is applicable for materials such as sintered SiC (v_{LSAW} = 6790 m/s, measured) and (111) diamond (v_{LSAW} = 10860 m/s, measured) with leaky SAW velocities much higher than 6000 m/s. The determination of velocity is, however, made directly from the dip intervals Δz in their $V_I(z)$ curves using (15), because only a few interference waves are obtained in the characterization region by the present line-focus beam with a half aperture angle of $\theta_M = 60°$.

Fig. 26 shows the relation of the theoretical and measured attenuation factors. In a region of relatively large attenuation ($\alpha = 1.0 \times 10^{-2} \sim 5.0 \times 10^{-2}$), the measured values are in good agreement with the theoretical values with the differences of several percent. As the attenuation becomes smaller, the difference grows larger and a typical difference is about 20 percent for leaky pseudo-SAW on (111) InSb. From experiments, there is a tendency for the difference to grow larger for materials with higher velocities (or higher acoustic impedances) and the measured values are likely to be smaller than the theoretical values. This might be attributed possibly to an increase in propagation loss in water due to dissolved air and a limitation of the measurement principle.

V. Discussion

A. Utilization Method

It has been satisfactorily demonstrated that the line-focus-beam acoustic microscope is a very useful system for quantitative material characterization. The system is applied to all sample configurations, such as semi-infinite, layered, or diffusion-layered, and thin-film structures, and it can detect all modes of leaky waves excited efficiently on the boundary. From the standpoint of making the most practical use of the system for material characterization, one should utilize the most dominant phenomenon of leaky wave modes on the boundary in order to obtain the greatest accuracy in measurement. Generally, a leaky SAW mode should be employed for most solids because it is the most fundamental mode. Where the leaky SAW does not exist or is not excited efficiently on the boundary, a leaky SSCW mode should be utilized alternatively. Thus, the two modes can cover most of a characterization area for solid materials through the $V(z)$ curve analysis. For $V(z)$ curves that are deformed due to multimode interference, one of the modes should be extracted clearly for characterizing materials according to the processing procedure of $V(z)$ curves.

Using the present measurement principle, the velocity and attenuation of related leaky modes are determined simultaneously. For materials that have homogeneous acoustic and structural properties, the velocity is the much more significant acoustic property for characterization than is attenuation, as it is less dependent on the acoustic frequency. It becomes very important to determine both the velocity and the attenuation for materials that have significant acoustic absorption or structural variations, such as surface roughness and material structures of grains, pores, and boundaries. These factors cause frequency dependence on the acoustic properties.

B. Measurement Accuracy

The measurement accuracy of the values for leaky waves should be examined. It is seen from (15) that in determining the velocity through the $V(z)$ curve analysis, the accuracy is affected by the three factors v_w, f, and Δz.

The measurement of the water temperature is made by a copper-constantan thermocouple. In the system a synthesized signal generator is used for experiments with resolution so sufficient that the frequency f has no influence on the measurement accuracy. The dip interval Δz will be affected by the precision of the mechanical translation, the alignment of the lens and samples, the electrical circuits, and processing errors in the analysis. The maximum error of the position may be considered to be ± 0.1 μm along the beam axis, it affects the measurement accuracy of the velocity by less than 0.01 percent. The error of the dip interval Δz, which is introduced by the other factors, is discussed here in experimental tests that determine the reliability of the measurement system and in the investigation of the attenuation.

Experiments were made in order to examine the reproducibility of measuring the acoustic properties of leaky SAW mode for a SiO_2 sample by repeated (about 200 times) alignment and arbitrarily positioning the sample. The velocity was distributed with a mean value of 3416 m/s and a standard deviation of 0.6 m/s. The attenuation yields a mean value of 3.85×10^{-2} and a standard deviation of 0.015×10^{-2}. These deviations are considered to be within about 0.02 percent for velocity and about 0.4 percent for attenuation, which is essential to the system and the analysis.

From these determinations, the overall relative measurement accuracy in the velocity can be estimated here to be better than 0.1 percent. With reference to the data obtained in Section IV-D, we believe that the absolute measurement accuracy might be better than ± 0.2 percent, considering the comparison between the measured and calculated values of leaky SAW's for α-quartz, Si, GGG, and sapphire, whose physical constants were measured with sufficient accuracy.

For the attenuation measurement, the absolute accuracy might depend upon the appropriate determination of the attenuation in water under the experimental conditions described in Section IV-D with errors from a few percent to about 20 percent, corresponding to the velocity of the materials.

C. Limitations

As the measurement principle requires a clear wave interference waveform in the $V(z)$ curves for determining the acoustic properties of leaky waves, the system employing water as a reference material has limitations for measuring materials. Specifically, it is required that the leaky waves must have the critical angles, given by $\theta_l = \sin^{-1}(v_w/v_l)$, within the half aperture angle of the lens and moderate normalized attenuation factors. In the case of water, measurements can be performed effectively for ma terials having the propagation characteristics of leaky waves with velocities v_l from about 1800 to 11000 m/s and a normalized attenuation factor from about 1×10^{-3} to 1×10^{-1}. To make more accurate measurements, it is desirable to select the lens with a suitable half aperture angle θ_M. A lens with $\theta_M = 30°$ is appropriate for materials with a velocity higher than 5000 m/s, $\theta_M = 60°$ for materials with a velocity range from 2000 to 6000 m/s, and $\theta_M = 70°$ for those from 1800 to 5000 m/s, taking into consideration the translation distance along the beam axis for the material characterization and the dip interval of the relevant leaky mode. It is a useful method to control the acoustic fields impinging on samples by selecting the electrode width of the acoustic transducer and by choosing the operating frequency [51]. However, for materials with a velocity lower than 1800 m/s, it becomes very difficult to measure the propagation properties using water as the reference fluid.

Other coupling liquids might make the $V(z)$ curve measurements more effective for materials with both higher and lower velocities than those given above. For mea-

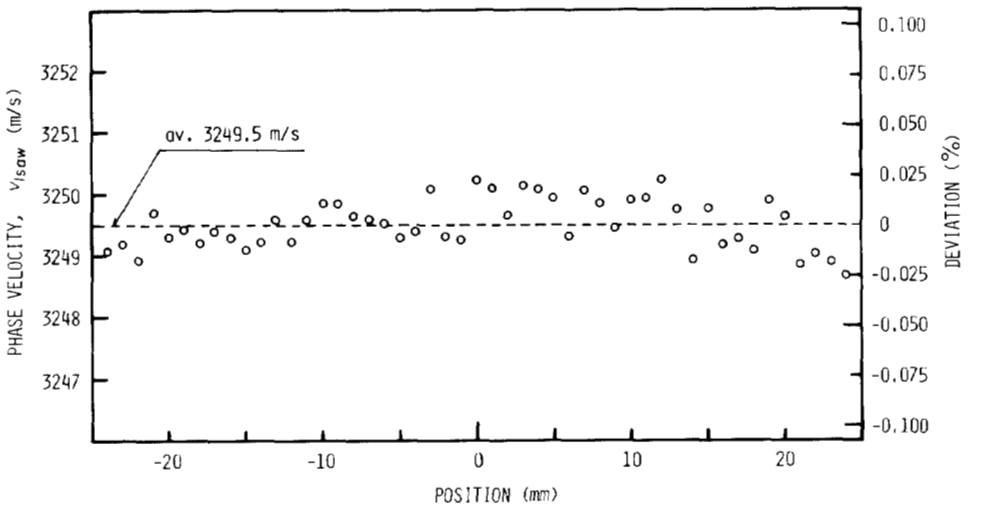

Fig. 27. Acoustic homogeneity in velocity on (111)-GGG wafer. The wave propaegates in the [110] direction.

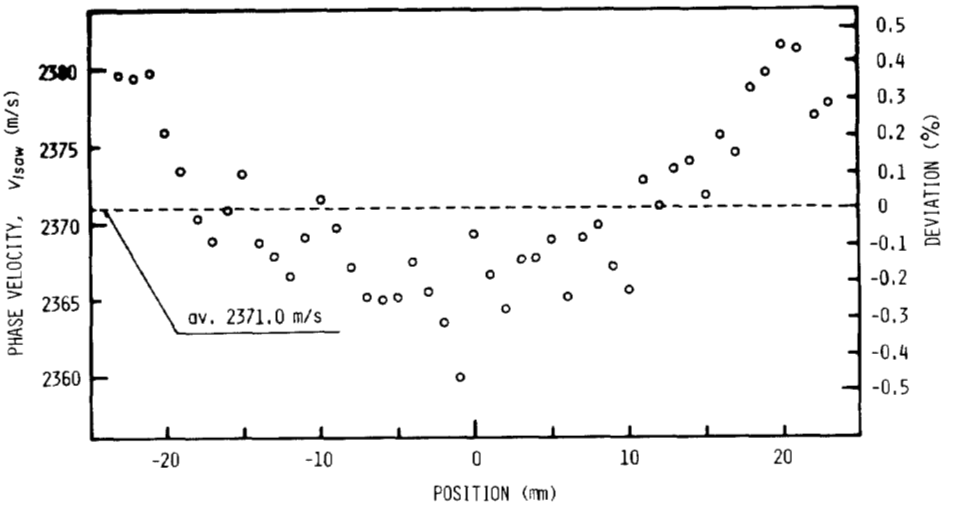

Fig. 28. Acoustic inhomogeneity in velocity on PZT ceramic wafer.

surements of materials with higher velocities than 6000 m/s, coupling could be achieved with liquid Ga (v_L = 2870 m/s and ρ = 6.1 × 10^3 kg/m^3 at 30°C). This is useful for the internal observation of solid devices [34]. On the other hand, for measurements of materials with lower velocities than 2500 m/s, we might select coupling liquids such as methyl alcohol (v_L = 1088 m/s and ρ = 781.8 kg/m^3 at 30°C) [52]; ethyl alcohol (v_L = 1134 m/s and ρ = 780.9 kg/m^3 at 30°C) [52]; a high pressure gas such as Ar (v_L = 323 m/s at 40 bar) [53]; and also liquid He (v_L = 238 m/s and ρ = 145 kg/m^3 at 0.2 K) [54]. Proper selection of coupling liquids as a reference material enables us to measure the leaky wave velocities for most of materials, although some of these coupling liquids are physically and chemically not as stable and easy to handle as water.

VI. Applications

A. Variation of Acoustic Properties on Wafers

The system has been applied in a preliminary fashion to investigate inhomogeneity of the acoustic velocities as a function of position. Examples of the studies that have been carried out are for a gadolinium gallium garnet (GGG) wafer (Shin-Etsu Chemical Company, Ltd.), which is well known as a substrate material needed for magnetic, bubble domain devices and is representative of a defect-free single crystal; and for a PZT ceramic wafer (Murata Manufacturing Company, Ltd.) with a grain size of 1 ~ 2 μm, which is used for surface wave filter devices.

Fig. 27 shows the experimental results measured for leaky SAW's propagating across the diameter, parallel to the [$\bar{1}$10] on a (111) GGG wafer of three inches in diameter. The excellent acoustical homogeneity is obtained with a mean value of v_{LSAW} = 3250 m/s with maximum differences of 0.05 percent. This also demonstrates the stability of the measurement system.

Similarly, Fig. 28 shows the results measured for a PZT ceramic wafer of two inches in diameter. As the line-focus beam has a uniform field distribution of about 1 mm along the line direction in water (see Fig. 10. (b)), which is much longer than the grain sizes of the sample, mean propagation characteristics of the leaky SAW can be mea-

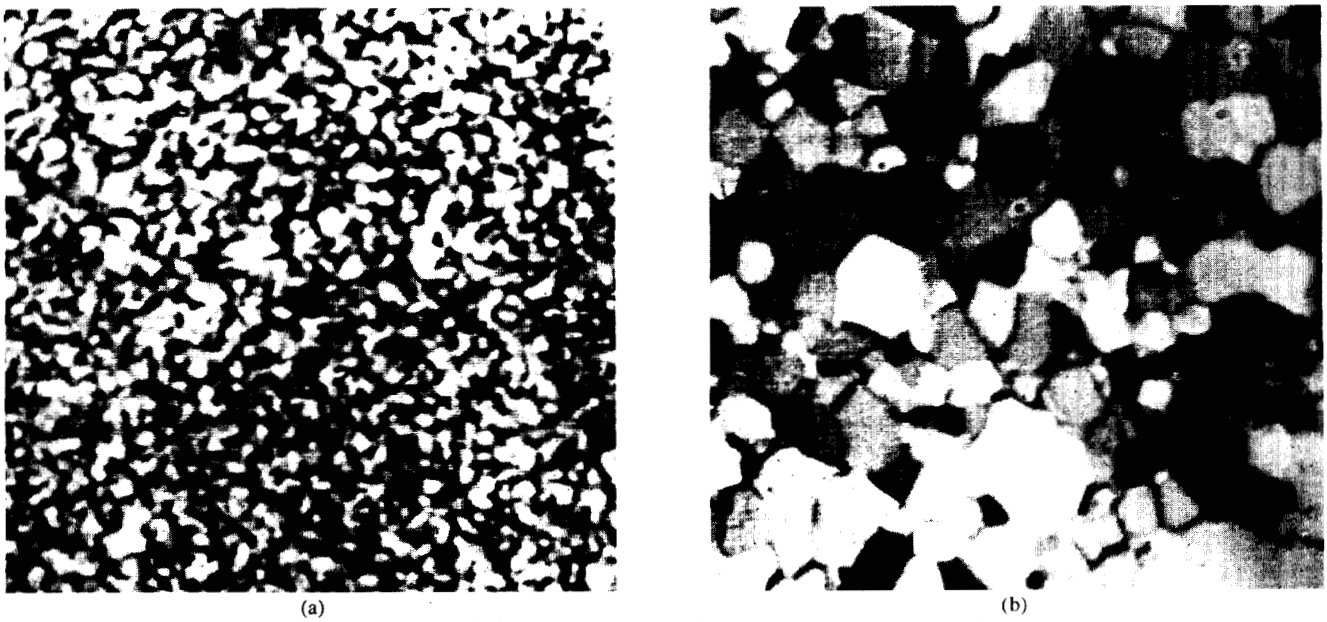

(a) (b)

Fig. 29. Acoustic images of Mn-Zn ferrite samples observed by the point-focus-beam acoustic microscope at 575 MHz (defocus: $z = -15$ μm). (a) Grain *S*. (b) Grain *L*.

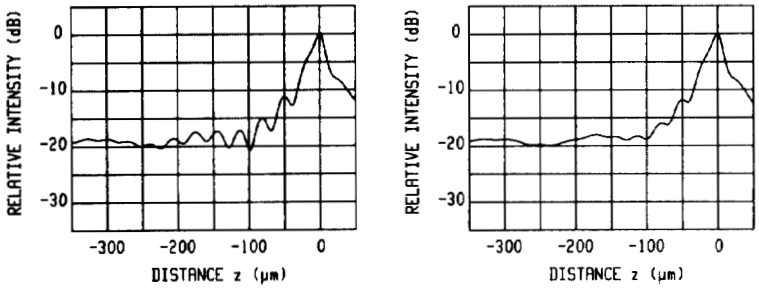

(a) (b)

Fig. 30. Measured $V(z)$ curves by the line-focus-beam acoustic microscope at 226.3 MHz for Mn-Zn ferrite samples shown in Fig. 29. (a) Grain *S*, (b) Grain *L*.

sured. It is shown that the velocities vary randomly with position and increase greatly in the radial direction. The mean velocity value of 2371 m/s with maximum differences of 0.9 percent was obtained. It seems that the variation is dependent on the distribution of different polycrystalline grains and slight surface roughness after poling, which can be observed on the surface of samples before poling.

B. Structural Analysis

In the case where the material characterization method is applied for materials with structural variations such as microscopic defects of grains, pores, and roughness near the surface, propagating waves on the boundary will be scattered, and this will be reflected in the $V(z)$ curves. Thus the system can detect information quantitatively on the surface condition of the sample and the distribution of such microscopic defects in the sample by extracting the attenuation due to the scattering effect from the measured total attenuation. On the other hand, such structures can be observed in an image as variations of acoustic properties by the point-focus-beam acoustic microscope with a resolution of less than one wavelength. So by combining quantitative macroscopic measurements with qualitative microscopic measurements, a new method of structural evaluation of solid materials may be established. This new method has been employed in an attempt to analyze the structural information on Mn–Zn ferrite materials for magnetic heads.

Fig. 29 shows the acoustic images for each sample observed by a scanning reflection acoustic microscope operating at a frequency of 575 MHz at defocus of $z = -15$ μm with a resolution of about 2 μm. Each sample has an average nominal grain size of 8 μm (grain *S* sample) and 50 μm (grain *L* sample), the surface of which is optically polished. From the photographs we can clearly recognize individual grains and boundaries with grains of $10 \sim 100$ μm in size for the grain *L* sample, while for the grain *S* sample we can see a distribution of smaller grains of several micrometers. The image is slightly blurred because of insufficient resolution.

Fig. 30 shows the typical $V(z)$ curves for each sample

TABLE V
ACOUSTIC PROPERTIES OF LEAKY SAW'S OBTAINED FOR MN-ZN FERRITE SAMPLES

Sample	Grain size (μm)	Phase velocity v_{LSAW} (m/s)	Normalized attenuation factor α_{LSAW}
Grain S	8	3317	3.68×10^{-2}
Grain L	50	3299	5.87×10^{-2}

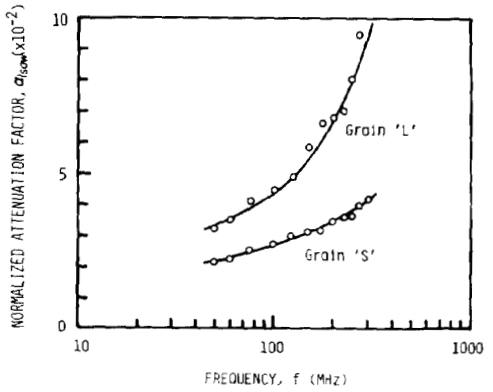

Fig. 31. Experimental results of frequency dependence of attenuation factor of leaky SAWs for Mn-Zn ferrite samples shown in Fig. 29.

measured by the acoustic line-focus beam at 226.3 MHz. It is easily seen from the interference phenomena in the $V(z)$ curves that the grain L sample has greater attenuation than does the grain S sample. The measured velocities and attenuations are given in Table V. The attenuation value for grain L sample is about 60 percent larger than that for the grain S sample, while the velocities for both samples are almost the same. This implies that the attenuation due to scattering at grain boundaries increases greatly with average grain sizes.

In order to study the frequency dependence of attenuation, we used three other lenses with a radius of 0.75, 1.25, and 1.5 mm. They are suitable for measurements from 50 to 300 MHz. In all cases the attenuation increased strongly with the frequency as shown in Fig. 31. Considering the variation of wavelength for the leaky SAW's with frequency, we believe that according to the scattering criteria [55] for the grain S sample, the scattering phenomenon for frequencies lower than 100 MHz are in the Rayleigh scattering region ($\lambda > 2\pi\bar{D}$ where $\bar{D}$ is the average grain sizes and λ is the wavelength). On the other hand, for the grain L sample, the phenomena are considered to be almost entirely in the intermediate region ($\lambda < 2\pi\bar{D}$).

In any case it is shown that quantitative measurements with the frequency dependence are expected to provide a useful means of analyzing the structure of materials by comparing results with acoustical imaging information observed by the point-focus-beam acoustic microscope.

VII. CONCLUSION

In this paper we have described a novel method of material characterization by using the line-focus-beam acoustic microscope. Material characterization has been made by quantitatively determining propagation characteristics, i.e., phase velocity and attenuation, of leaky waves on the water–sample boundary through $V(z)$ curve measurement. In order to measure the two acoustic quantities from the measured $V(z)$ curves, a general measurement principle has been developed with a simple model derived from a combination of ray and field theories. We have shown that $V(z) = V_I(z) + V_L(z)$, where $V_I(z)$ and $V_L(z)$ are the interference output and the characteristic lens response, respectively. The principle has been expanded for the interference associated with multiple leaky waves. Spectral analysis has been introduced as a general means of analyzing the $V_I(z)$ curves. In the spectrum distribution that is obtained with the Fourier transform, the velocity is determined from a center frequency which gives a maximum spectrum, while the attenuation is determined from a spread of spectra. The line-focus-beam acoustic microscope system, which was developed here with the software implementation of the measurement procedure, has been applied to a variety of solid materials. Both isotropic and anisotropic materials with velocities ranging from 2000 to 11000 m/s have been measured. It has been shown that the system can detect propagation characteristics and anisotropy for all leaky wave modes, such as leaky SAW, leaky pseudo-SAW, leaky SSCW, leaky Lamb wave, and haromic waves, that are excited efficiently on the boundary. It has been estimated here that the absolute measurement accuracy is about ± 0.2 percent for the velocity measurements (better than 0.1 percent for relative measurements) and from a few percent to 20 percent for the attenuation measurements.

The following is summarized from these investigations that the line-focus-beam acoustic microscope has several distinctive features of interest.

1) The system is suitable for quantitative measurements of the acoustic properties of materials, including anisotropy, because of the directionality of the acoustic line-focus beam.
2) Propagation characteristics for only desired leaky wave modes can be extracted from $V(z)$ curves.
3) A proper model can be established for the theoretical and experimental investigations.
4) The results obtained with the line-focus beam are available for basic investigations in order to interpret acoustic images obtained by the point-focus beam.

Two possible applications of the material characterization method have been demonstrated in a preliminary fashion. One example has been shown for detecting acoustic inhomogeneities on wafers used for electronic materials, such as (111) GGG and PZT ceramics. The system has revealed the homogeneity in elastic property on the GGG wafer and the marked variations on the PZT ceramics wafer that are mainly due to the distribution of different polycrystalline grains and slight surface rough-

ness. It is suggested that quantitative information of such acoustic properties may be displayed in a picture mapped as a function of position on wafers for practical application. Another example has been the preliminary use of a new method for combining the quantitative measurements made with the line-focus-beam acoustic microscope with the acoustical imaging measurements obtained with the point-focus-beam acoustic microscope.

One of the most valuable applications of the system would be for determining material constants by computer-fitting the precisely measured propagation characteristics of relevant leaky wave modes for bulk as well as thin-film materials grown on substrates. This study will be reported in detail elsewhere. In the near future, the line-focus-beam acoustic microscope system is expected to play an important role in the fields of material science as well as nondestructive and noncontacting evaluation.

Acknowledgments

The authors are very grateful to T. Sannomiya for his helpful discussions and technical assistance on experimental instruments throughout this work and to A. Ohkubo, H. Maehara, K. Horii, and Y. Matsumoto for their invaluable support in experiments and calculations in their M.E. graduate course. The authors wish to express their thanks to many persons who cooperated by supplying samples: S. Morita at Tohoku University for Ge and InSb; Y. Ohmachi at the Musashino Electrical Communication Lab. for vitreous As_2S_3 and As_2Se_3; Prof. K. Ishii at Nagoya Institute of Technology for Pb; K. Yamanaka at the Mechanical Engineering Lab. for sintered SiC and diamond; Y. Tanihara and N. Horie at Takasaki Works, Hitachi Ltd. for Si and GaAs; A. Fukumoto at Matsushita Electric Industrial Co. Ltd. for tellurite glass; O. Kamata at Matsushita Electric Industrial Co. Ltd. and H. Goto at Fuji Electrochemical Co. Ltd. for YIG; M. Sugimura at Matsushita Electric Industrial Co. Ltd. and U. Kato at Tohoku Metal Industries Ltd. for Mn-Zn ferrite samples; and M. Kadota at Murata Mfg. Co. Ltd. for PZT ceramics. The authors would like to thank M. Aihara for the X-ray analysis.

References

[1] R. A. Lemons and C. F. Quate, "A scanning acoustic microscope," in *Proc. 1973 IEEE Ultrason. Symp.*, pp. 18–20, 1973.

[2] C. F. Quate, A. Atalar, and H. K. Wickramasinghe, "Acoustic microscope with mechanical scanning—a review," *Proc. IEEE*, vol. 67, pp. 1092–1114, Aug. 1979.

[3] ——, "Phase imaging in reflection with the acoustic microscope," *Appl. Phys. Lett.*, vol. 31, pp. 791–793, Dec. 1977.

[4] A. Atalar, "An angular-spectrum approach to contrast in reflection acoustic microscope," *J. Appl. Phys.*, vol. 49, pp. 5130–5139, Oct. 1978.

[5] H. K. Wickramasinghe, "Contrast and imaging performance in the scanning acoustic microscope," *J. Appl. Phys.*, vol. 50, pp. 664–672, Feb. 1979.

[6] ——, "Contrast in reflection acoustic microscopy," *Electron. Lett.*, vol. 14, pp. 305–306, May 1978.

[7] R. D. Weglein, "A model for predicting acoustic material signatures," *Appl. Phys. Lett.*, vol. 34, pp. 179–181, Feb. 1979.

[8] W. Parmon and H. L. Bertoni, "Ray interpretation of the material signature in the acoustic microscope," *Electron. Lett.*, vol. 15, pp. 684–686, Oct. 1979.

[9] A. Atalar, "A physical model for acoustic signatures," *J. Appl. Phys.*, vol. 50, pp. 8237–8239, Dec. 1979.

[10] R. D. Weglein and R. G. Wilson, "Characteristic material signatures by acoustic microscopy," *Electron. Lett.*, vol. 14, pp. 352–354, June 1978.

[11] R. C. Bray, C. F. Quate, J. Calhoun, and R. Koch, "Film adhesion studies with the acoustic microscope," *Thin Solid Films*, vol. 74, pp. 295–302, Dec. 1980.

[12] K. Yamanaka, Y. Enomoto, and Y. Tsuya, "Application of scanning acoustic microscope to the study of fracture and wear," in *Acoustical Imaging*, E. A. Ash and C. R. Hill, Eds. New York: Plenum, 1982, vol. 12, pp. 79–87.

[13] M. G. Somekh, G. A. D. Briggs, and C. Ilett, "The effect of elastic anisotropy on contrast in the scanning acoustic microscope," *Phil. Mag.*, vol. 49, pp. 179–204, Feb. 1984.

[14] R. Hammer and R. L. Hollis, "Enhancing micrographs obtained with a scanning acoustic microscope using false-color encoding," *Appl. Phys. Lett.*, vol. 40, pp. 678–680, Apr. 1982.

[15] R. D. Weglein, "Rayleigh wave absorption via acoustic microscopy," *Electron. Lett.*, vol. 18, pp. 20–21, Jan. 1982.

[16] K. Yamanaka, "Analysis of SAW attenuation measurement using acoustic microscopy," *Electron. Lett.*, vol. 18, pp. 587–589, May 1982.

[17] J. Kushibiki, A. Ohkubo, and N. Chubachi, "Linearly focused acoustic beams for acoustic microscopy," *Electron. Lett.*, vol. 17, pp. 520–522, July 1981.

[18] ——, "Anisotropy detection in sapphire by acoustic microscope using line-focus beam," *Electron. Lett.*, vol. 17, pp. 534–536, July 1981.

[19] ——, "Propagation characteristics of leaky SAWs on water/$LiNbO_3$ boundary measured by acoustic microscope with line-focus beam," *Electron. Lett.*, vol. 18, pp. 6–7, Jan. 1982.

[20] J. Kushibiki, K. Horii, and N. Chubachi, "Leaky SAW velocity on water/silicon boundary measured by acoustic line-focus beam," *Electron. Lett.*, vol. 18, pp. 732–734, Aug. 1982.

[21] J. Kushibiki, A. Ohkubo, and N. Chubachi, "Theoretical analysis for $V(z)$ curves obtained by acoustic microscope with line-focus beam," *Electron. Lett.*, vol. 18, pp. 663–664, July 1982.

[22] ——, "Theoretical analysis of $V(z)$ curves measured by acoustic line-focus beam," in *Proc. 1982 IEEE Ultrason. Symp.*, pp. 623–628, 1982.

[23] ——, "Material characterization by acoustic microscope with line-focus beam," in *Acoustical Imaging*, E. A. Ash and C. R. Hill, Eds. New York: Plenum, 1982, vol. 12, pp. 101–111.

[24] ——, "Effect of leaky SAW parameter on $V(z)$ curves obtained by acoustic microscopy," *Electron. Lett.*, vol. 18, pp. 668–670, July 1982.

[25] J. Kushibiki, K. Horii, and N. Chubachi, "Multimode interference mechanism in $V(z)$ curves obtained by acoustic line-focus beam," *Electron. Lett.*, vol. 19, pp. 359–361, May 1983.

[26] ——, "Velocity measurement of multiple leaky waves on germanium by line-focus-beam acoustic microscope using FFT," *Electron. Lett.*, vol. 19, pp. 404–405, May 1983.

[27] J. Kushibiki, Y. Matsumoto, and N. Chubachi, "Attenuation measurements of leaky waves by the acoustic line-focus beam," *Electron. Lett.*, vol. 19, pp. 512–514, July 1983.

[28] M. Greenspan and C. E. Tschiegg, "Speed of sound in water by a direct method," *J. Res. Nat. Bur. Stand.*, vol. 59, pp. 249–254, Oct. 1957.

[29] H. L. Bertoni and T. Tamir, "Unified theory of Rayleigh-angle phenomena for acoustic beams at liquid-solid interfaces," *J. Appl. Phys.*, vol. 2, pp. 157–172, 1973.

[30] J. M. M. Pinkerton, "The absorption of ultrasonic waves in liquids and its relation to molecular constitution," *Proc. Phys. Soc.*, vol. B20, pp. 129–141, Feb. 1949.

[31] C. F. Quate, "Microwaves, acoustics and scanning microscopy," *Scanned Image Microscopy*, E. A. Ash, Ed. New York: Academic, 1980, pp. 23–55.

[32] M. Takeuchi and H. Shimizu, "Leaky Lamb waves in a solid plate with water loading on its one surface," *J. Acoust. Soc. Japan*, vol. 32, pp. 420–429, July 1976.

[33] D. L. Waldorf and G. A. Alers, "Low-Temperature Elastic Moduli of Lead," *J. Appl. Phys.*, vol. 33, pp. 3266–3269, Nov. 1962.

[34] J. Attal, "Acoustic microscopy: imaging microelectronic circuits with liquid metals," *Scanned Image Microscopy*, E. A. Ash, Ed. New York: Academic, 1980, pp. 97–118.

[35] Y. Ohmachi and N. Uchida, "Investigation of acousto-optical properties and application to infrared modulator," *J. Appl. Phys.*, vol. 43, pp. 1709–1712, Apr. 1972
[36] J. Mort, "Elastic constants of trigonal selenium," *J. Appl. Phys.*, vol. 38, pp. 3414–3415, July 1967.
[37] G. S. Kell, "Density, thermal expansivity, and compressibility of liquid water from 0° to 150°C: correlations and tables for atmospheric pressure and saturation reviewed and expressed on 1968 temperature scale," *J. Chem. Eng. Data*, vol. 20, pp. 97–105, 1975.
[38] M. Greenspan and C. E. Tschiegg, "Effect of dissolved air on the speed of sound in water," *J. Acoust. Soc. Am.*, vol. 28, p. 501, 1956.
[39] J. Kushibiki, H. Maehara, and N. Chubachi, "Acoustic properties of evaporated chalcogenide glass films," *Electron. Lett.*, vol. 17, pp. 322–323, Apr. 1981.
[40] Y. Torikai, "Ultrasonic fields and Lommel's functions," *Report of the Institute of Industrial Science*, University of Tokyo, vol. 25, Mar. 1976.
[41] J. Kushibiki, T. Sannomiya, and N. Chubachi, "A useful acoustic measurement system for pulse mode in VHF and UHF range," *IEEE Trans. Sonics Ultrason.*, vol. SU-29, pp. 338–342, Nov. 1982.
[42] J. J. Campbell and W. R. Jones, "Propagation of surface waves at the boundary between a piezoelectric crystal and a fluid medium," *IEEE Trans. Sonics Ultrason.*, vol. SU-17, pp. 71–76, Apr. 1970.
[43] R. Bechman, "Elastic and piezoelectric constants of alpha-quartz," *Phys. Rev.*, vol. 110, pp. 1060–1061, June 1958.
[44] J. Kushibiki, Y. Matsumoto, and N. Chubachi, "Material characterization by acoustic line-focus beam," in *Acoustical Imaging*, M. Kaveh, R. K. Mueller, and J. F. Greenleaf, Eds. New York: Plenum, 1984, pp. 193–202.
[45] B. A. Auld, *Acoustic Fields and Waves in Solids*. New York: John Wiley & Sons, 1976, chap. 3, p. 96.
[46] E. M. Conwell, "Properties of silicon and germanium," *Proc. IRE*, vol. 50, pp. 1327–1337, Nov. 1952.
[47] J. B. Wachtmann, Jr., W. E. Tefft, D. G. Lam, Jr., and R. P. Stinchfield, "Elastic constants of synthetic single crystal corundum at room temperature," *J. Res. Nat. Bur. Stand.*, vol. 64A, pp. 213–228, May–June 1960.
[48] W. P. Mason, *Physical Acoustics and the Properties of Solids*, New York: McGraw-Hill, 1958, p. 17.
[49] A. J. Slobodnik, Jr., E. D. Conway, and R. T. Delmonico, "Microwave acoustics handbook (Vol. 1A: Surface wave velocities)," USAF Cambridge Res. Labs., AFCRL-TR-73-0597, 1973.
[50] A. W. Warner, M. Onoe, and G. A. Coquin, "Determination of elastic and piezoelectric constants for crystals," *J. Acoust. Soc. Amer.*, vol. 42, pp. 1223–1231, Dec. 1967.
[51] J. Kushibiki, Y. Matsumoto, and N. Chubachi, "Effects of acoustic field distribution of line-focus beam on $V(z)$ curves," in *Proc. Acoust. Soc. Japan*, pp. 661–662, Mar. 1983.
[52] R. A. Lemons and C. F. Quate, "Acoustic microscopy," *Physical Acoustics*, W. P. Mason and R. N. Thurston, Eds. New York: Academic, 1979, pp. 1–92.
[53] H. K. Wickramasinghe and C. R. Petts, "Gas medium acoustic microscopy," *Scanned Image Microscopy*, E. A. Ash, Ed. Academic, 1980, pp. 57–70.
[54] D. Rugar, J. S. Foster, and J. Heisermann, "Acoustic microscopy at temperature less than 0.2 K," in *Acoustical Imaging* E. A. Ash and C. R. Hill, Eds. New York: Plenum, 1982, vol. 12, pp. 13–25.
[55] E. P. Papadakis, "Ultrasonic attenuation caused by scattering in polycrystalline media," in *Physical Acoustics* W. P. Mason, Ed. New York: Academic, vol. 4, Part B, chap. 15, pp. 269–328, 1968.
[56] T. Yano, A. Fukumoto, and A. Watanabe, "Tellurite glass: a new acousto-optics materials," *J. Appl. Phys.*, vol. 42, pp. 3674–3676, Sept. 1971.

Jun-ichi Kushibiki (M'83) was born in Hirosaki, Japan, on November 23, 1947. He received the B.S., M.S., and Ph.D. degrees in electrical engineering from Tohoku University, Sendai, Japan, in 1971, 1973, and 1976, respectively.

In 1976 he became a Research Associate at the Research Institute of Electrical Communication, Tohoku University. Since 1979 he has been at the Department of Electrical Engineering, Faculty of Engineering, Tohoku University. He has been engaged in the studies of acoustooptic interactions, piezoelectric thin-film materials and ultrasonic transducers, and acoustic microscopy. In the past four years he has concentrated his attention on material characterization by the line-focus-beam microscope.

Dr. Kushibiki is a member of the Institute of Electronics and Communication Engineers of Japan, the Acoustical Society of Japan, and the Japan Society of Ultrasonics in Medicine.

Noriyoshi Chubachi (M'83) was born in Kokura, Japan, on October 5, 1933. He received the B.S., M.S., and Ph.D. degrees in electrical engineering from Tohoku University, Sendai, Japan, in 1956, 1962, and 1965, respectively.

In 1965 he joined the Research Institute of Electrical Communication, Tohoku University, where he was an Associate Professor from 1966 to 1978. Since 1979 he has been a Professor at the Department of Electrical Engineering, Tohoku University. From 1982 to 1983 he was a visiting Professor of Electrical and Computer Engineering, University of California, Santa Barbara, CA. He has worked on ultrasonic transducers and delay lines, surface acoustic devices, acoustoelectronics, piezoelectric materials, acoustic microscopy, and related problems.

Dr. Chubachi is a member of the Institute of Electronics and Communication Engineers of Japan, the Society of Japanese Applied Physics, the Acoustical Society of Japan, the Japan Society of Ultrasonics in Medicine, and the Japan Society for Nondestructive Inspection.